AD A069671

CONTRACT REPORT ARBRL-CR-00395

ENERGY DENSITY CALCULATIONS: DIPOLE WEST SHOT 11

Prepared by

University of Victoria
Victoria, British Columbia
Canada, V8W 2Y2

April 1979

US ARMY ARMAMENT RESEARCH AND DEVELOPMENT COMMAND
BALLISTIC RESEARCH LABORATORY
ABERDEEN PROVING GROUND, MARYLAND

Approved for public release; distribution unlimited.

Destroy this report when it is no longer needed.
Do not return it to the originator.

Secondary distribution of this report by originating or sponsoring activity is prohibited.

Additional copies of this report may be obtained from the National Technical Information Service, U.S. Department of Commerce, Springfield, Virginia 22161.

The findings in this report are not to be construed as an official Department of the Army position, unless so designated by other authorized documents.

The use of trade names or manufacturers' names in this report does not constitute indorsement of any commercial product.

UNCLASSIFIED

SECURITY CLASSIFICATION OF THIS PAGE *(When Data Entered)*

REPORT DOCUMENTATION PAGE

READ INSTRUCTIONS BEFORE COMPLETING FORM

1. REPORT NUMBER: CONTRACT REPORT ARBRL-CR-00395
2. GOVT ACCESSION NO.:
3. RECIPIENT'S CATALOG NUMBER:

4. TITLE *(and Subtitle)*: ENERGY DENSITY CALCULATIONS: DIPOLE WEST SHOT 11

5. TYPE OF REPORT & PERIOD COVERED: Final Report: 29 September 1977 through 29 March 1978

6. PERFORMING ORG. REPORT NUMBER:

7. AUTHOR(s): J. M. Dewey and D. J. McMillin

8. CONTRACT OR GRANT NUMBER(s): DAK 11-77-C-0110
Canadian GE Contract No. 9509-50417

9. PERFORMING ORGANIZATION NAME AND ADDRESS:
University of Victoria
Victoria, British Columbia
Canada, V8W 2Y2

10. PROGRAM ELEMENT, PROJECT, TASK AREA & WORK UNIT NUMBERS:

11. CONTROLLING OFFICE NAME AND ADDRESS:
General Electric Company—TEMPO
7800 Marble Avenue NE, Suite 5
Albuquerque, N.M. 87110

12. REPORT DATE: APRIL 1979

13. NUMBER OF PAGES: 43

14. MONITORING AGENCY NAME & ADDRESS *(if different from Controlling Office)*:
USA Ballistic Research Laboratory
DRDAR-BLT, COR: Ralph E. Reisler
Aberdeen Proving Ground, Md 21005

15. SECURITY CLASS *(of this report)*: UNCLASSIFIED

15a. DECLASSIFICATION/DOWNGRADING SCHEDULE:

16. DISTRIBUTION STATEMENT *(of this Report)*:
Approved for public release; distribution unlimited.

17. DISTRIBUTION STATEMENT *(of the abstract entered in Block 20, if different from Report)*:

18. SUPPLEMENTARY NOTES:

19. KEY WORDS *(Continue on reverse side if necessary and identify by block number)*:
Air Blast
Energy Density
Simultaneous Detonations
Multiburst Detonations

20. ABSTRACT *(Continue on reverse side if necessary and identify by block number)*:
DIPOLE WEST/11 comprised the simultaneous detonation of two 490-kg spherical charges of Pentolite. The particle trajectories in the resulting blast waves were measured, using the high-speed photography of smoke puffs, and analyzed. In this report, the results of the particle trajectory analysis are used to calculate energy densities within the blast waves. Energy density profiles and integrated energy yields for the primary spherical blast wave from the lower charge are presented and compared to energy density profiles and

DD FORM 1 JAN 73 1473 EDITION OF 1 NOV 65 IS OBSOLETE

UNCLASSIFIED

SECURITY CLASSIFICATION OF THIS PAGE *(When Data Entered)*

20. ABSTRACT (continued)

integrated energy yields calculated using the theoretical results of Brode, which describe a single charge of TNT detonated in the absence of a reflecting surface. Agreement is found to be good within the limits of uncertainty placed on the experimental and theoretical results. Energy profiles through the Mach stem blast waves above the ground and beneath the dipole interaction plane are also presented. The total energy within the leading portion of these waves is computed at several times and, in each case, the energy in the wave above the ground is found to be greater than that in the wave beneath the interaction plane. The total amount of energy in the Mach stem wave at the ground is also found to increase with time. These results may be explained by the lack of symmetry in the dipole configuration at greater distances from the charges. It is recommended that attempts be made to improve the particle trajectory analysis techniques in order to increase the accuracy of the energy measurements, thus leading to more conclusive results.

TABLE OF CONTENTS

LIST OF ILLUSTRATIONS

1. INTRODUCTION

The analysis of particle trajectories in blast waves from dipole explosions has been described by Dewey et al (1977a, 1977b, 1978a, and 1978b). The experiments in which particle trajectory measurements were made, referred to as DIPOLE WEST Shots 8, 9, 10 and 11, were designed to provide information on the interaction of spherical blast waves with real and ideal reflecting surfaces. The blast wave interactions were obtained by the simultaneous detonation of two identical 490-kg spherical Pentolite charges placed one above the other such that the distance between the charges was equal to twice the height of the lower charge above the ground surface.

Two different charge heights were used over two different types of ground surface. The lower charge was 25 feet above the ground in Shots 8 and 11 and 15 feet in Shots 9 and 10. For Shots 8 and 9 the ground surface was relatively smooth, and for Shots 10 and 11 the ground surface was roughened by ploughing.

Two photogrammetrical studies were made in each of the four experiments. One study permitted a calculation of the shock front trajectories and velocities, and subsequently a determination of the physical properties immediately behind the shocks (Dewey et al, 1975). The other study involved the high-speed photography of an array of smoke puffs, which permitted the determination of the particle trajectories within the blast waves. These trajectories were analyzed to provide the space and time variations of particle velocity, gas density, hydrostatic overpressure, dynamic pressure and total pressure within the waves.

This report presents the energy densities within the blast waves of Shot 11, computed using the particle trajectory data obtained as described above. Shot 11 was chosen for this initial study of energy density because of the charge positions and the ground surface which were used. The charge positions were such that a larger amount of data was obtained for the primary, spherical blast wave from the lower of the two charges than was obtained with the closer charge spacing of Shots 9 and 10.

The ground surface for Shot 11 was rough, and the strength of the Mach stem shock over the rough ground surface was found to be significantly less than that of the Mach stem shock at the interaction plane between the two charges, and less than that of the Mach stem shock over the smooth ground surface of Shot 8. This difference in strength is presumably due to energy losses and redistribution over the rough ground. The more extensive smoke puff grid used for Shot 11 yielded nearly twice the amount of data in the Mach wave as was obtained for Shot 10, which also used a rough ground surface.

A complete description of DIPOLE WEST Shot 11 and the photogrammetric measurements made can be found in Dewey et al, 1975, 1977a, 1977b, 1978a, and 1978b.

2. CALCULATION OF ENERGY DENSITY

The available energy per unit volume at a point in a blast wave may be computed using the following equation:

$$E = \frac{1}{\gamma - 1} (P - P_a) + \tfrac{1}{2} \rho u^2 \qquad (1)$$

where P is the hydrostatic pressure of the gas, P_a the ambient hydrostatic pressure before the arrival of the blast wave, ρ the gas density, u the velocity of the gas, and γ the ratio of specific heats for the gas. The parameters P, ρ and u vary with both position and time.

All of the calculations described in this report were made using data which were scaled to 1-kg charges detonated in a standard atmosphere. The values of the hydrostatic pressure difference $(P - P_a)$ were computed using the hydrostatic overpressure ratios obtained from particle trajectory analysis multiplied by the standard pressure, $P_a = 101.324$ kPa. Values of gas density, ρ, and particle velocity, u, may be obtained by multiplying the density ratios and particle velocity Mach numbers obtained from the particle trajectory analysis by the standard density $D_a = 1.225$ kg/m^3 and the standard sound speed $C_a = 340.292$ m/s, respectively. In fact, since dynamic pressure ratios $(\gamma/2)(\rho/D_a)(u/C_a)^2$ had already been computed as part of the particle trajectory analysis, the second term in equation (1) was calculated by multiplying the dynamic pressure ratio by $D_a C_a^{\,2}/\gamma$. A value of 1.401 was used for γ assuming that the shock waves were relatively weak and thus produced no real gas effects.

Energy density values computed in the above manner were divided by 10^6 to have units of Joules per cubic centimeter. As computed, they measure the available energy above the internal energy of the ambient air. Integrated over the entire blast wave, the total energy thus measured should equal the energy yield of the charge in megaJoules when the distance coordinate is measured in meters. Since the results of the particle trajectory analysis were scaled to a standard charge weight and standard atmospheric conditions, the energy densities presented in this report describe the case of two 1-kg charges detonated in a standard atmosphere at sea level at 15°C.

To obtain results describing the original event, DIPOLE WEST Shot 11, the distance values presented in this report should be multiplied by 8.0730, and the time values by 8.5933. The values of energy density do not require scaling. Energy data are presented in this report as functions of either radial position or position along a line, at fixed times. The data can, on request, also be given as energy density

contours over a regular, two-dimensional Eulerian grid at specified times, or as energy density time histories at specified positions.

3. THEORETICAL RESULT FOR A SPHERICAL WAVE FROM TNT (BRODE)

To validate the equation used to compute energy density (equation (1) in the preceding section) and to have standard curves against which to compare experimentally determined energy density profiles, a set of energy density versus distance curves was prepared using data computed theoretically by Brode (1957) for TNT. Brode's calculation produced curves showing particle velocity Mach number, β; hydrostatic pressure ratio, π, and gas density ratio, η, as functions of reduced radius, λ, at various reduced times, τ, for a spherical TNT blast wave in a standard atmosphere (sea level) at 0°C.

Curves of energy density versus distance from charge center were computed using Brode's results in the following equation:

$$E = \frac{1}{\gamma - 1} (\pi - 1) P_o + \tfrac{1}{2} \eta D_o (\beta C_o)^2 , \qquad (2)$$

where P_o, D_o and C_o are the ambient values of atmospheric pressure, density and sound speed used by Brode, which are slightly different from the values P_a, D_a and C_a given in the previous section. Again, a value of 1.4 was assumed for γ. A value of 1 cm was chosen for Brode's scaling factor, α, and the computed energy density functions were integrated over the full sphere of the blast wave at selected times, using

$$E_{TOT} = 4\pi \int_o^R r^2 E(r) dr ,$$

where R is the primary shock radius. Results of the integrations are given below.

Brode's Reduced time value, τ	Integrated Energy E_{TOT}, Joules
0.08577	0.08169
0.12216	0.07771
0.14793	0.08576
0.21564	0.06761
	mean = 0.0782 J

Since Brode's scaling factor is defined by $\alpha^3 = W/P_o$, where W is the total energy released by the charge, choosing a value of 1 cm for the scaling factor should have been equivalent to setting the energy yield of the charge in Brode's calculation at $W = \alpha^3 P_o = 0.1014$ J.

It is not clear that this figure is the one to expect from the integrations described above, however, as Brode arbitrarily added a fixed amount of energy in his equation of state for TNT to overcome difficulties he had in reconciling the integral of that equation to the total energies expected under various initial and limiting conditions.

In order to validate the equation used to compute energy densities for this report, therefore, a second approach was taken. A scaling factor of $\alpha = 3.966$ m was applied to Brode's reduced radius values, λ, to obtain energy results for a 1-kg charge in a standard atmosphere at 15°C. This scaling factor was computed using a factor of 10 feet derived empirically by Dewey (1964).

The scaling factor of 10 feet was found to give the best agreement between Brode's computed peak overpressure-versus-distance relationship and similar values for TNT, which have been measured experimentally and scaled to a 1-lb charge weight in Brode's standard atmosphere. This factor of 10 feet was converted to meters and then multiplied by $\sqrt[3]{2.20462}$ to convert from 1 lb to 1 kg, then by the cube root of the ratio P_o/P_a to convert from Brode's standard atmosphere (0°C) to the standard atmosphere used in this report (15°C). Brode's reduced time values, τ, were scaled using this same factor, divided by the standard sound speed at 15°C, then multiplied by 1000 to obtain real times, t, in milliseconds.

The resulting energy density profiles are shown in Figure 1, where energy density in J/cm^3 is plotted versus radius in meters, scaled to a 1-kg charge, at the following times: 1.000, 1.424, 1.725, 2.514, 3.413, 5.918, and 8.532 ms. A curve showing peak energy density versus radius is also shown.

To validate this method of computing energy densities, the data presented in Figure 1 were integrated over the full sphere of the blast wave. The results obtained are as follows:

Time (ms)	Energy (MJ)
1.000	5.097
1.424	4.848
1.725	5.351
2.514	4.218
3.413	(5.282)
5.918	(3.488)
8.532	(2.835)

The energy values shown in parentheses do not represent total energy

because energy density was not defined over the full range of radii between the explosion center and the primary shock front. The results of the other integrations, which were made over the full range of radii, are total energies varying from 4.218 to 5.351 MJ with a mean value of 4.878 MJ. These results should be compared to the total energy yield of 1 kg TNT, which is thought to be in the range from 4.45 to 4.85 MJ.

The expected yield from 1 kg TNT was estimated using Brode's figures (from Jones and Miller, 1948) of 247.9 kcal/mole at a loading density of 1.5 g/cm^3 and molecular weight of 234 g. These figures give a yield for TNT of 1.06 kcal/g, which can be compared to 1.16 kcal/g used by Dewey (1964), based on data from Cook (1958) for a loading density of 1.57 g/cm^3. These two figures, as lower and upper limits, and a conversion rate of 4185 J/kcal, put the yield of 1 kg TNT between 4.45 and 4.85 MJ. For comparison, the yield from 1 kg Pentolite (50/50) is approximately 5.10 MJ, and the yield from 1 kg TNT computed using the relation $W = \alpha^3 P_a$, $\alpha = 3.966$ m , is 6.32 MJ.

4. PRIMARY WAVE FROM THE LOWER CHARGE: DIPOLE WEST/11

DIPOLE WEST Shot 11 involved the simultaneous detonation of two 490-kg spheres of Pentolite over a rough ground surface on 8 November 1973. The lower charge was positioned 25 feet above the ground and the upper charge 50 feet above the lower one. In this way, the spherical primary blast wave from the lower charge was reflected both from the ground surface and from the corresponding blast wave generated by the upper charge along an interaction plane midway between the two charges at a distance above the lower charge equal to the height of the lower charge above the ground. One objective of the experiment was to compare the Mach stem blast wave over the ground surface with the corresponding Mach stem wave below the interaction plane.

The region in space affected by the spherical primary wave from the lower charge is shown in Figure 2. The plane of the figure is one containing the two charge centers and ground zero. The x-coordinate is measured horizontally from ground zero and the y-coordinate vertically upward from ground zero. The distance units have been scaled to a 1-kg charge and standard atmospheric conditions, as described by Dewey et al (1978b). The region of the primary wave is bounded by the paths of the two triple points, that is, the trajectories of the junctions of the primary shock with the reflected shocks from the ground and the interaction plane.

The positions of the primary shock front and its upper and lower reflections at times 1.0, 1.4, 1.7, 2.5 and 3.4 ms are also shown in Figure 2. These times were chosen to correspond to the times at which theoretical results were computed from Brode's data.

Particle trajectory analysis using smoke puff flow tracers in the

plane of Figure 2 has provided a grid of measured particle velocities, gas densities, and hydrostatic overpressures in a region which overlaps the region of the primary wave between the triple point paths (Dewey et al, 1978b). These data were used to compute a regular grid of energy density values. Energy densities computed in the region of the primary wave are plotted in Figures 3 to 7 as functions of radial distance from the lower charge center at each of the times indicated in Figure 2. The solid curves shown in Figures 3 to 7 are the profiles computed using Brode's theoretical data. The vertical line represents the shock front position at the indicated time. The peak value of the energy density at the shock front (the height of the vertical line) was computed using the Rankine-Hugoniot equations and the measured shock velocity which were obtained as part of the particle trajectory analysis (Dewey et al, 1978b).

A position within the region bounded by the triple point paths may have been traversed by the primary shock only, or the primary shock and one reflected shock, or the primary shock and two reflected shocks. In Figures 3 to 7, the points corresponding to these conditions are represented as solid, or open containing a short vertical line, or open containing a cross, respectively. Only the solid points should be compared with the curves computed using Brode's data.

The fields of energy density may be conceptualized as three dimensional surfaces over the x-y plane, as described by Dewey et al (1977a). Cross-sections of these surfaces along a line $y = 0.9$ m (the charge height) are indicated by dashed lines in Figures 5 to 7.

The scatter in the energy density values computed in the regions behind one or two reflected shocks (Figures 5 to 7) is to be expected because the flows in these regions do not have the spherical symmetry which was assumed when the data were plotted versus radial distance from the charge center. Additional scatter within each region, including the region affected by the spherical primary wave only (Figures 3 to 7), arises from scatter in the gas density calculations, which is inherent in the method used to derive gas density from observed particle trajectories. Attempts are being made to improve this method of deriving gas density.

5. ANOTHER PRIMARY WAVE: FE589/6

One of the difficulties encountered in deriving energy density in the primary wave from the lower charge in DIPOLE WEST Shot 11 is the scarcity of data which have been unaffected by a reflected wave, especially at later times. A particle trajectory analysis was therefore made of another explosion, FE589 Shot 6, which offered larger amounts of data in the primary wave unaffected by a reflected shock.

FE589 Shot 6 was a 1000-lb sphere of TNT detonated on 17 October

1969 at a height of 60 feet. Because of the large charge height and the positioning of the smoke puff grid, a relatively large amount of particle trajectory data was obtained for the primary blast wave. Also, since there was only one charge, there was only one reflection.

Profiles of energy density in the primary wave from FE589 Shot 6 are shown in Figures 8 to 11 at times 2.514, 3.413, 5.918 and 8.532 ms, along with the curves computed using Brode's data at those times. The profiles shown in Figures 8 to 11 are similar to those shown in Figures 3 to 7 for DIPOLE WEST Shot 11, with the solid points representing energy density at positions affected by only the primary wave, and the open points with a small vertical line representing energy density at positions affected by both the primary and the reflected wave. With the exception of the open points in Figure 11, the values plotted in Figures 8 to 11 were derived for a region which would be expected to have spherical symmetry, and the scatter of the results is primarily caused by the lack of precision in determining gas density from the particle trajectories. The shock front positions and peak energy densities shown in Figures 8 to 11 were computed from shock front trajectory data obtained using refractive image analysis. The relationship between the peak energy densities computed using refractive image analysis and those computed from times of arrival derived using particle trajectory analysis is shown in Figure 12, along with the same curve derived from Brode's data.

6. MACH STEM ENERGY PROFILES: DIPOLE WEST/11

Energy profiles of the Mach stem blast waves above the ground surface and beneath the interaction plane between the two charges are presented in Figures 13 to 17. In these figures, energy density is plotted against a radial distance which is measured horizontally from the axis through the two charge centers and ground zero, at heights of 0.4 m above the ground and 0.4 m below the interaction plane. Plotting the energy data in this way assumes that the flows within the Mach stem blast waves are cylindrically radial, an assumption which is known to be only approximate, as discussed by Dewey et al (1977a). The profiles for the two blast waves in each figure are plotted at different times chosen so that the shock fronts were at the same radial distance. This was necessary because the shock wave beneath the interaction plane was traveling faster than the one above the ground. Thus, for example, in Figure 13 the shocks are both at a radius of 3.52 m, which occurred at 4.8 ms for the interaction Mach stem, and at 5.0 ms for the ground Mach stem.

The peak energy density at each shock front was calculated using the measured shock velocities, and for all values of shock radius it was greater for the shock below the interaction plane than for the shock at the ground surface. The exact relationship between the strength of the Mach stem beneath the interaction plane and the Mach stem at the

ground surface is shown in Figures 18 and 19, as determined using refractive image analysis and particle trajectory analysis, respectively.

The Mach stem shock below the interaction plane is apparently stronger than the Mach stem shock over the ground surface when peak energy densities at the shock fronts are compared. Such a difference is not apparent when the energy density profiles of the waves behind the shock fronts are compared (Figures 13 to 17). The energy densities in the wave above the ground surface are, if anything, greater than those in the wave beneath the interaction plane.

Values of the integral $2\pi\int_{r_o}^{R} rE(r)dr$, where r_o is the radius marked by an arrow in Figures 13 to 17, and R is the shock front radius, are as follows:

INTEGRATED ENERGY DENSITY (MJ/m)

Figure Number	Interaction Mach Stem	Ground Mach Stem
13	3.00	2.90
14	3.06	3.78
15	3.45	4.11
16	3.52	4.72
17	3.55	5.29

If these integrated values are taken as true measures of the total energy in megaJoules per meter of distance from the reflecting surfaces, over those portions of the waves indicated in Figures 13 to 17, then indeed the wave over the ground surface appears to be the more energetic. This would be consistent with the results reported by Dewey et al (1975) and Keefer et al (1975), in which it was shown that, although the peak hydrostatic pressure was always less above the ground than close to the interaction plane at the same radial distance, the pressure impulse, namely the integral of the pressure-time history, was always greater in the ground Mach stem.

The integrations of energy listed above also suggest that in the leading portion of the ground Mach wave, the total energy may increase with time, whereas in the corresponding portion of interaction Mach wave, the total energy remains more or less constant.

Unfortunately, the scatter in the values of energy density plotted in the profiles is such that no firm conclusions can be drawn. As discussed previously, this scatter arises primarily because of the poor spatial resolution of the density calculated from the particle trajectories, and it is hoped that techniques can be developed to improve this feature of the analysis.

7. CONCLUSIONS

This report describes the first attempt to calculate the energy density throughout a blast wave using experimentally determined properties of the gas, viz, density, pressure, and particle velocity. The energy density is the most complete descriptor of a blast wave since it involves all of these physical properties. In addition, an integration of the energy density profile should produce a total energy equivalent to that released by the explosion, less any energy losses by such means as thermal radiation and seismic effects. The integration for the total energy release can thus provide a means of checking all previously computed results.

Attempts were made to validate the method used to calculate the energy densities presented in this report, but these attempts were not entirely successful. The most complete theoretical description of a blast wave from a spherical chemical source is that given for TNT by Brode (1957). Energy density profiles were calculated from Brode's data at several times and integrated to give a total energy yield. Using an arbitrary value of 1 cm for Brode's scaling factor, the energy profile was integrated at four different times to give values of total energy in the range from 0.06761 J to 0.08576 J with a mean of 0.0782 J. These figures may be compared with Brode's supposed energy yield of 0.1015 J. The 25-percent difference may possibly be accounted for by the fact that, in the integration, a constant ratio of specific heats was used, and no allowance was made for varying the equation of state of the detonation products. Brode found it necessary to add energy to his equation of state to overcome this difficulty.

As a final approach to the problem of validation, Brode's data were scaled so that they would describe a 1-kg charge of TNT in standard atmospheric conditions, using an empirical scaling factor obtained by matching the shock front pressure-distance relationship of Brode to that determined experimentally for TNT. Integrating these data gave a mean energy yield of 4.878 MJ ($\pm$ 0.566), which may be compared with energies in the range from 4.45 to 4.85 MJ that were obtained from various other sources as the expected energy release from 1 kg TNT.

These studies bring to light the limitations in our knowledge of the absolute energy release from a chemical explosive. It appears, however, that the methods described here for determining the energy density profile in a blast wave, and its integration, are valid and provide answers which are correct to better than order-of-magnitude accuracy.

The energy density profile was determined in the primary shock wave from the lower charge of DIPOLE WEST Shot 11. There was a considerable scatter in the results because many were for positions also affected by one or two reflected shocks. The results for positions affected only by the primary shock show reasonable agreement with the

energy profiles calculated from Brode's data.

In order to obtain results for a primary shock region less affected by reflected shocks, a similar analysis was carried out for the blast wave from a 1000-lb TNT charge detonated at a height of 60 feet (FE589/6). These results show similar agreement with the energy density profiles computed using Brode's data, but again contain a large amount of scatter. It is believed that this scatter arises primarily from the method used to determine gas density from the experimentally observed particle trajectories, and it is hoped that the prerequisite calculation can be improved.

The comparisons of the energy density profiles in the Mach stem regions of DIPOLE WEST Shot 11, shown in Figures 13 to 17, are not entirely conclusive due to the scatter in the results. As was previously known from the shock front analyses, the Mach stem shock close to the ground is always weaker than the Mach stem shock at the interaction plane, at equal distances from the central axis of symmetry. However, as previously reported, the pressure impulses obtained by integrating pressure gauge signals are always greater close to the ground. This last result is confirmed by the present results in that the integrated energy densities for the profiles shown in Figures 13 to 17 are always greater in the ground Mach stem than in the interaction Mach stem. This is a surprising result in that it might be expected that there would be some energy losses to the ground. A possible explanation may come from the fact that the region below the interaction plane in the dipole configuration of the charges is no longer symmetrical beyond a certain horizontal distance (a scaled horizontal distance of approximately 4.2 m). Referring to Figure 2, the reflected shock beneath the upper triple point path will be reflected from the ground and pass through the trailing part of the Mach stem wave above the ground, adding energy to this wave. The corresponding reflected shock above the lower triple point path will not encounter an equivalent wave from the upper charge and will therefore pass through the interaction plane without adding energy to the Mach stem wave below the interaction plane.

These results cannot be considered conclusive at the present time, however, since the accuracy of the measurements may not warrant any such distinction between the two sets of energy profiles; and it may be only coincidence that the integrals of the energy profiles along the ground were greater than those beneath the interaction plane in each of the five cases considered.

It is recommended that attempts be made to resolve this question, by improving the accuracy of the energy calculations and by further studies of the energy density profiles in these and other blast waves.

REFERENCES

Brode, H.L., *U.S. Air Force Research Memorandum*, ASTIA Report No. AD 144302, 1957.

Cook, M.A., *The Science of Explosives*, Reinhold Publishing Corporation, New York, 1958.

Dewey, J.M., "The Air-Velocity and Density in Blast Waves from TNT Explosions," *Proc. Roy. Soc., A 279*, pp. 366-385, 1964.

Dewey, J.M., D.F. Classen, and D.J. McMillin, *Photogrammetry of the Shock Front Trajectories on DIPOLE WEST Shots 8, 9, 10, and 11*, DNA 3777F, 1975.

Dewey, J.M., D.J. McMillin, and D. Trill, *Photogrammetry of Particle Trajectories on DIPOLE WEST Shots 8, 9, 10, and 11*. Published in five volumes, specifically as follows:

Volume 1, Shot 10, DNA 4326F-1, 1977. (Ref., Dewey et al, 1977a)

Volume 2, Shot 9, DNA 4326F-2, 1977. (Ref., Dewey et al, 1977b)

Volume 3, Shot 8, DNA 4326F-3, 1978. (Ref., Dewey et al, 1978a)

Volume 4, Shot 11, DNA 4326F-4, 1978. (Ref., Dewey et al, 1978b)

Volume 5, Comparison of Results, DNA 4326F-5 (in press).

Jones, H., and A.R. Miller, "The Detonation of Solid Explosives: The Equilibrium Conditions in the Detonation Wave-Front and the Adiabatic Expansion of the Products of Detonation," *Proc. Roy. Soc. 194*, pp. 480-507, 1948.

Keefer, J.H., and R.E. Reisler, *Multiburst Environment—Simultaneous Detonations, Project DIPOLE WEST*, BRL Report R1766, 1975. (AD #A009485)

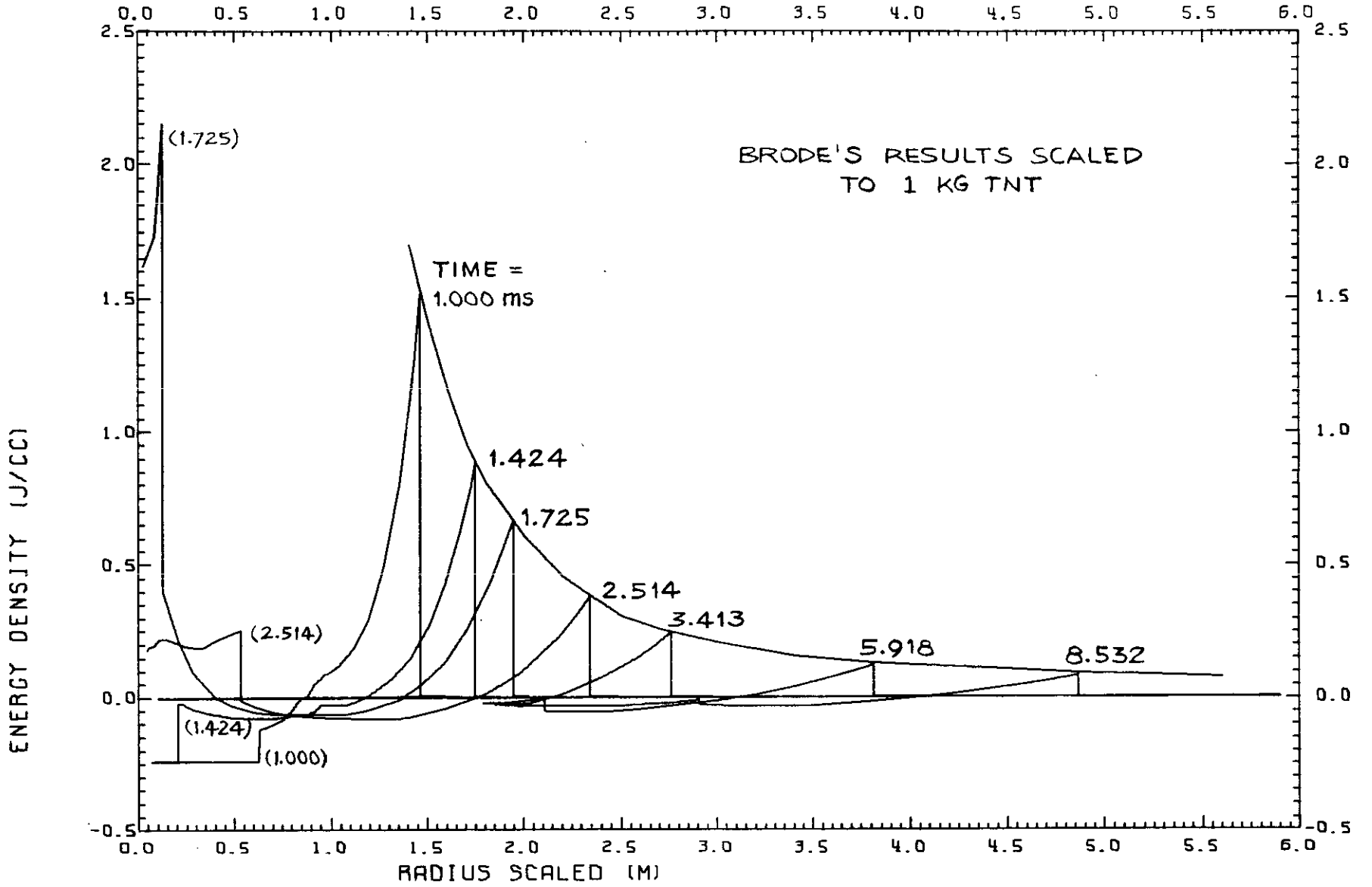

Figure 1 - Energy density curves for TNT, from Brode

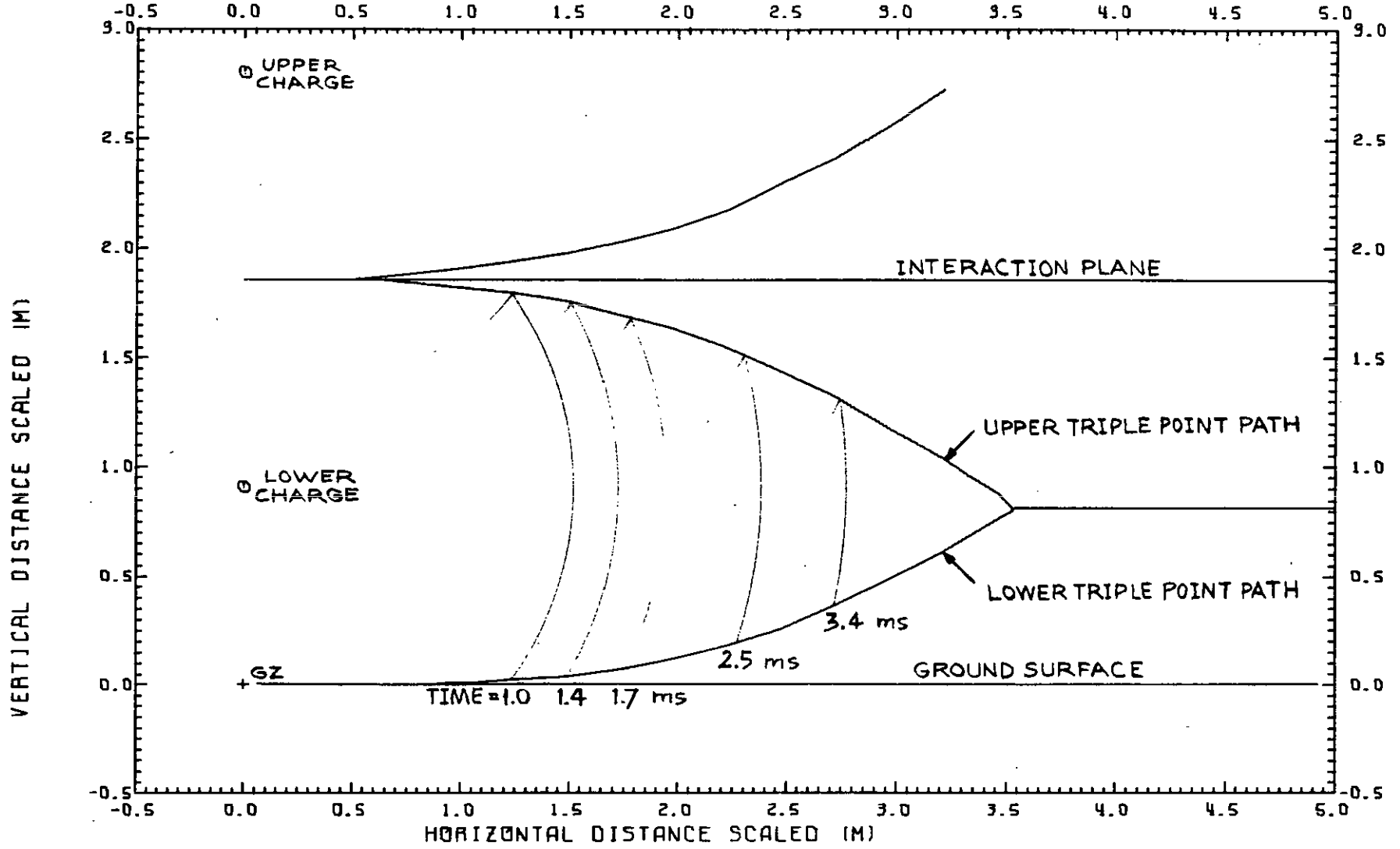

Figure 2 - Region of primary waves from lower charge, Dipole West/11

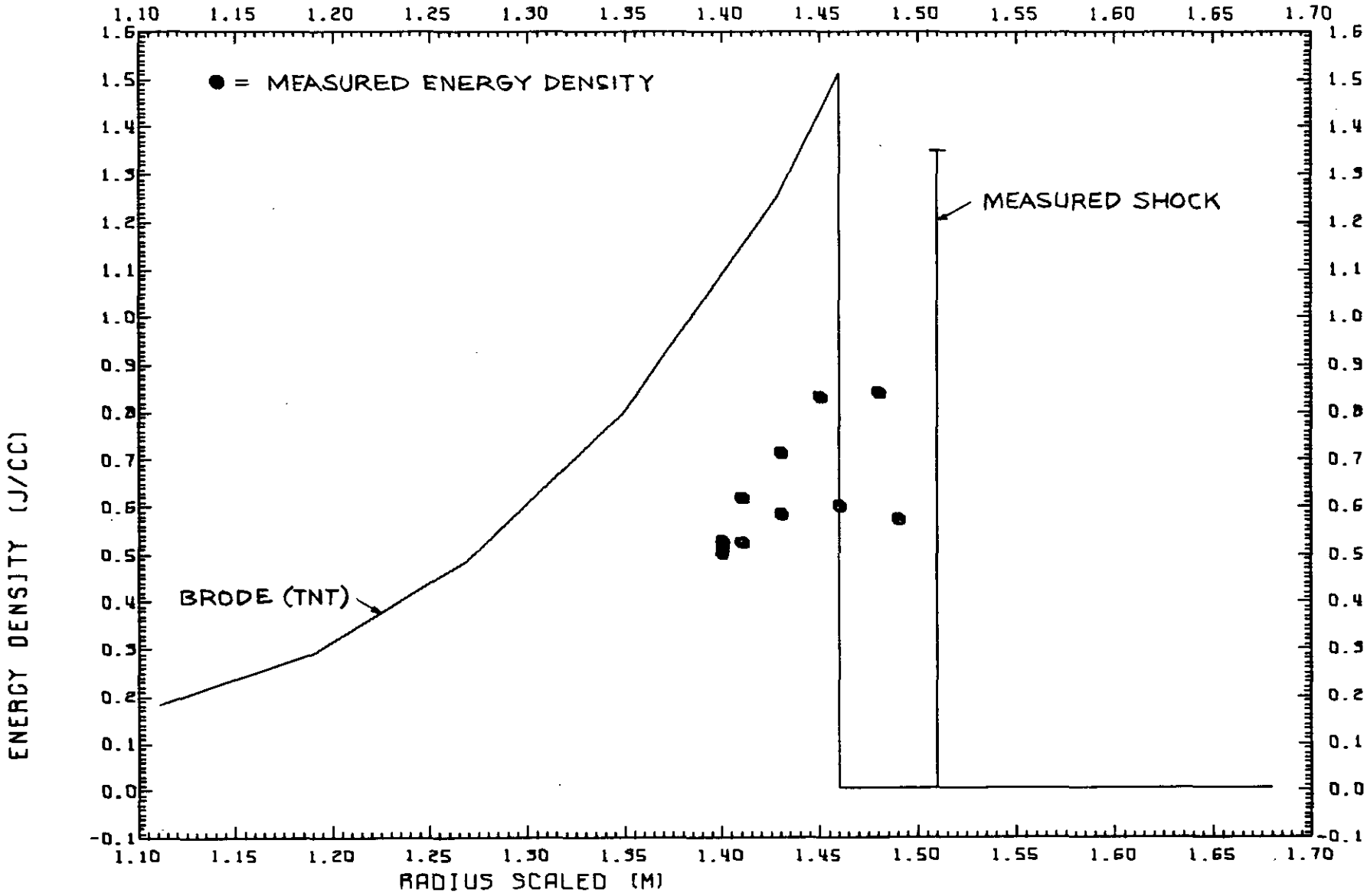

Figure 3 - Energy density in the primary wave, Dipole West/11 (t = 1.0 ms)

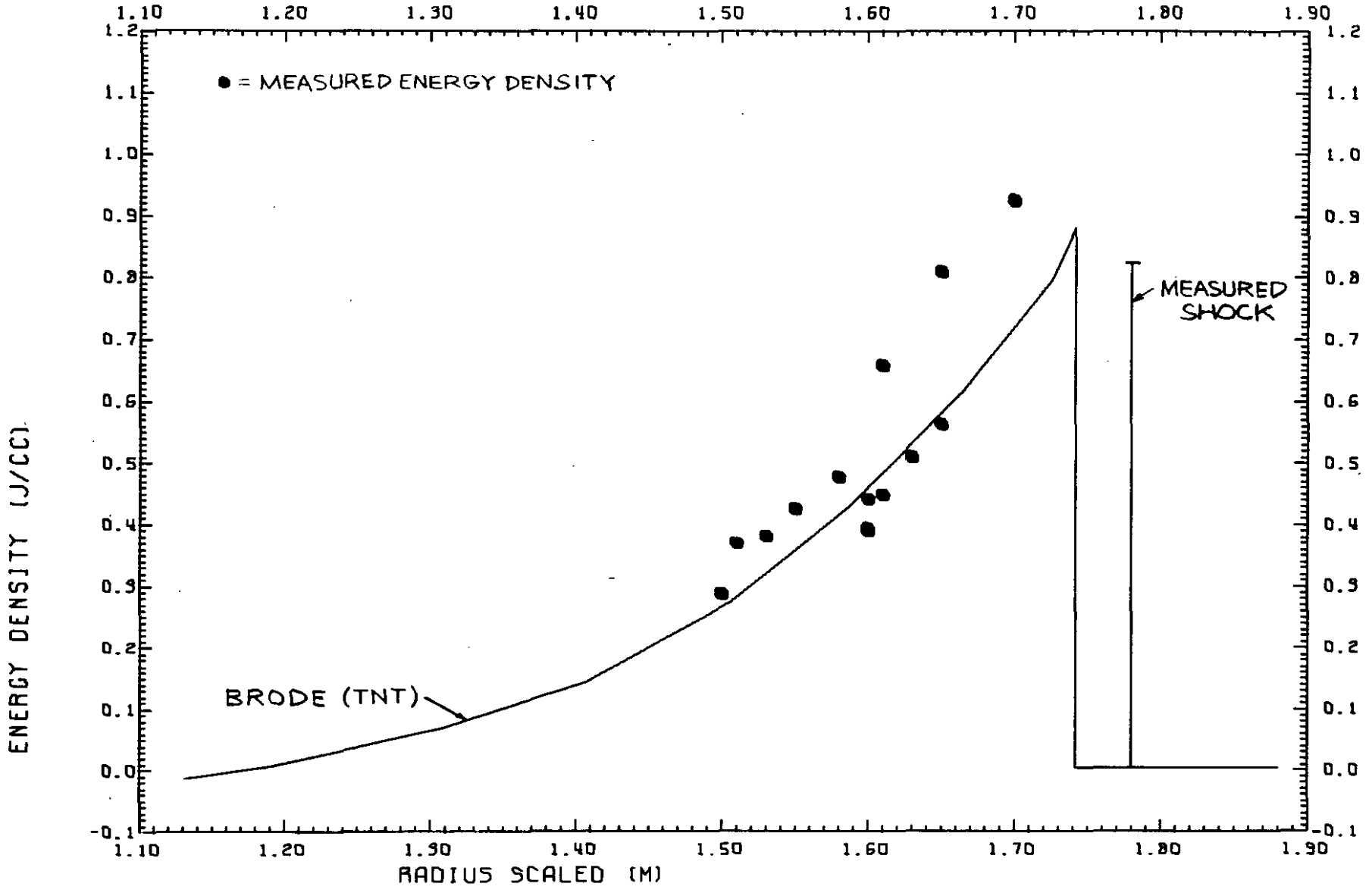

Figure 4 - Energy density in the primary wave, Dipole West/11 (t = 1.4 ms)

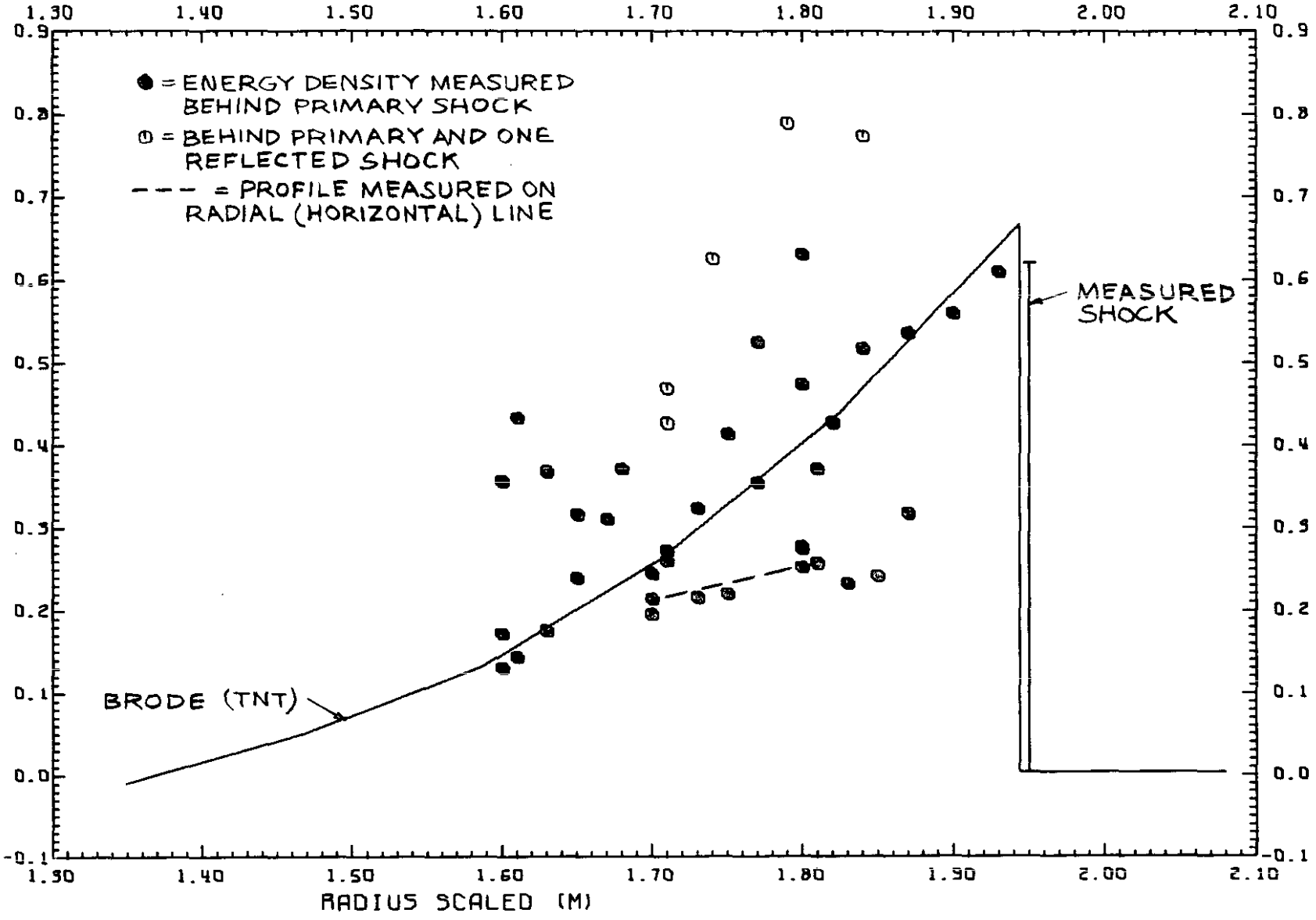

Figure 5 - Energy density in the primary wave, Dipole West/11 (t = 1.7 ms)

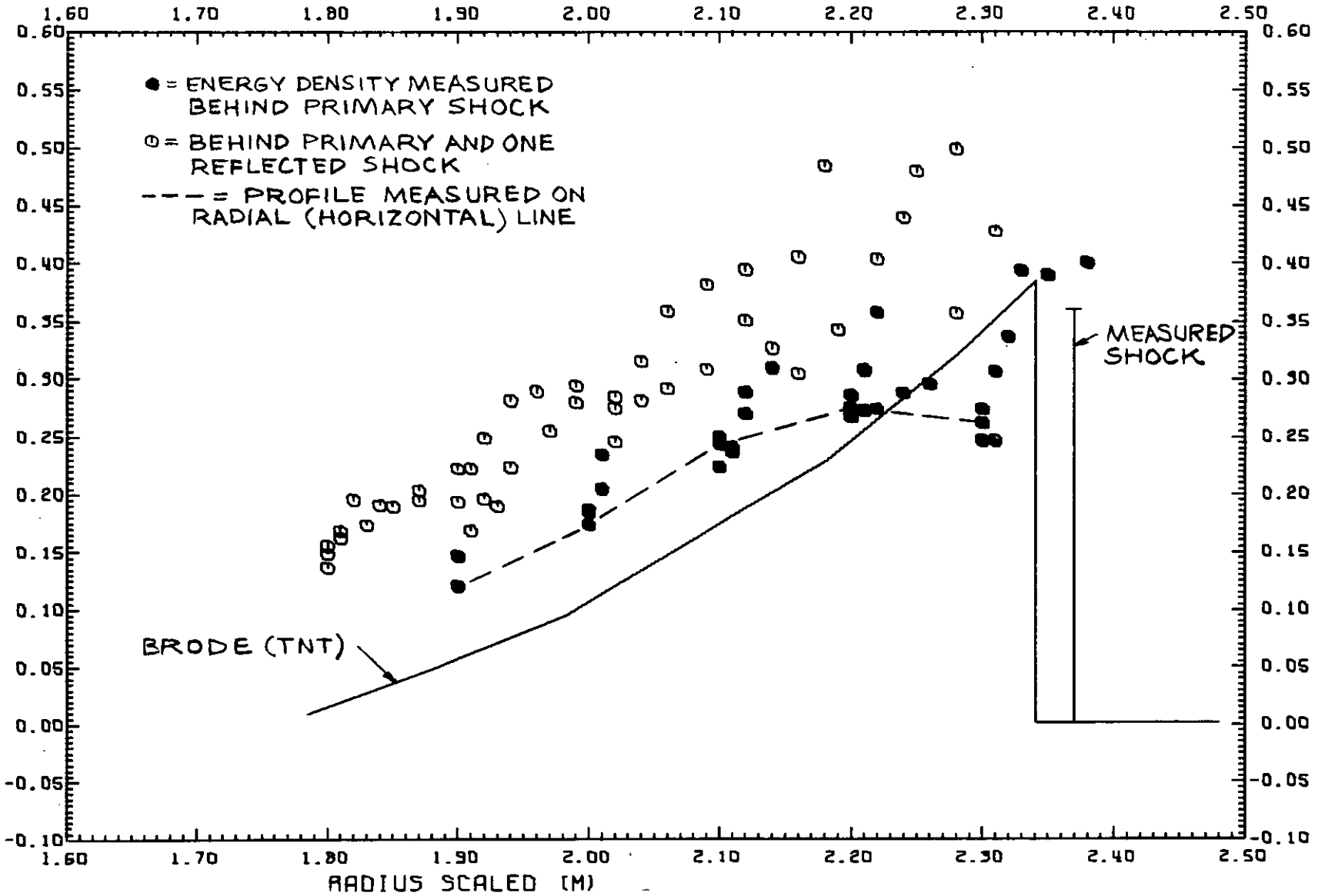

Figure 6 - Energy density in the primary wave, Dipole West/11 (t = 2.5 ms)

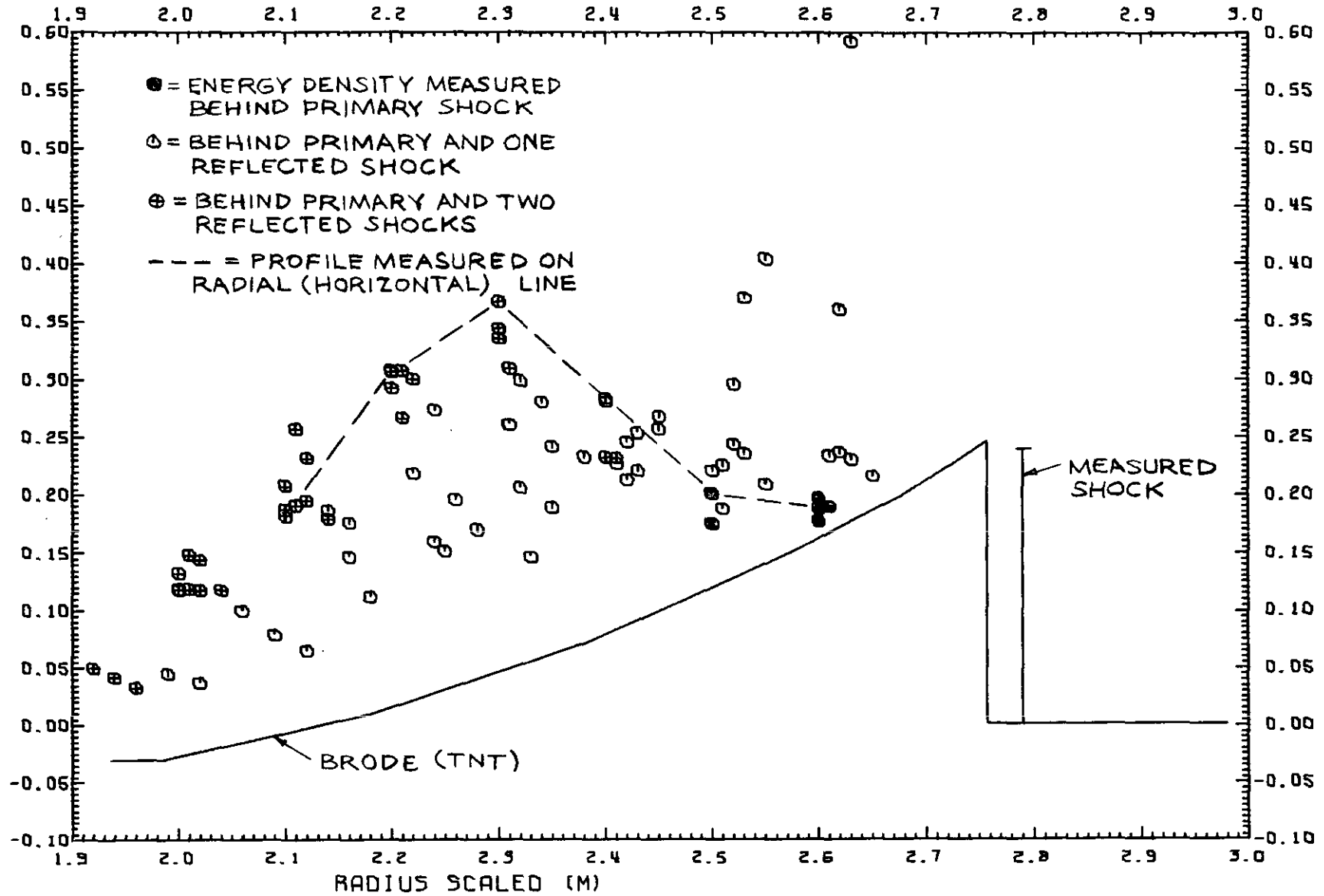

Figure 7 - Energy density in the primary wave, Dipole West/11 (t = 3.4 ms)

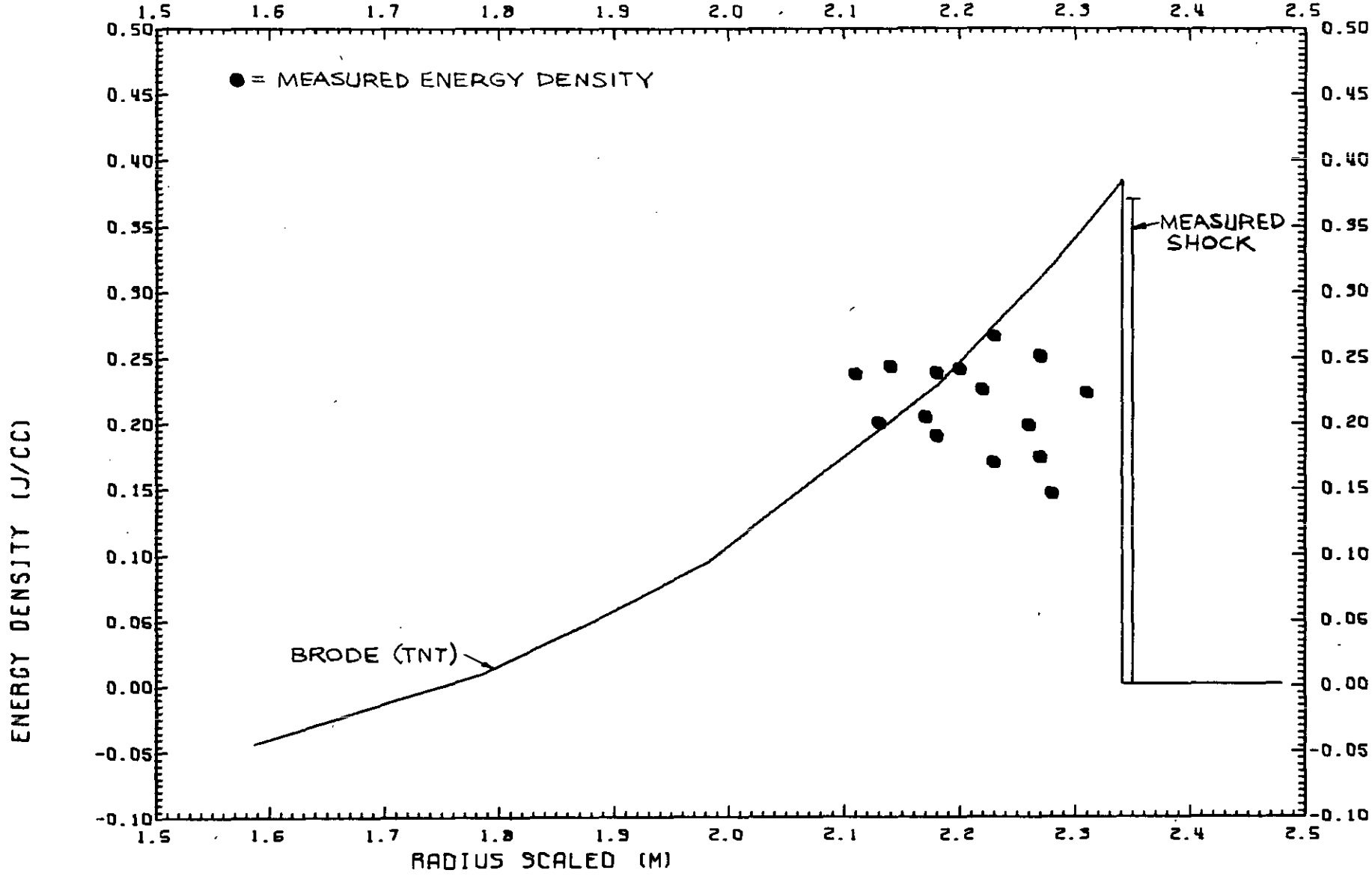

Figure 8 - Energy density in the primary wave, FE589/6 (t = 2.514 ms)

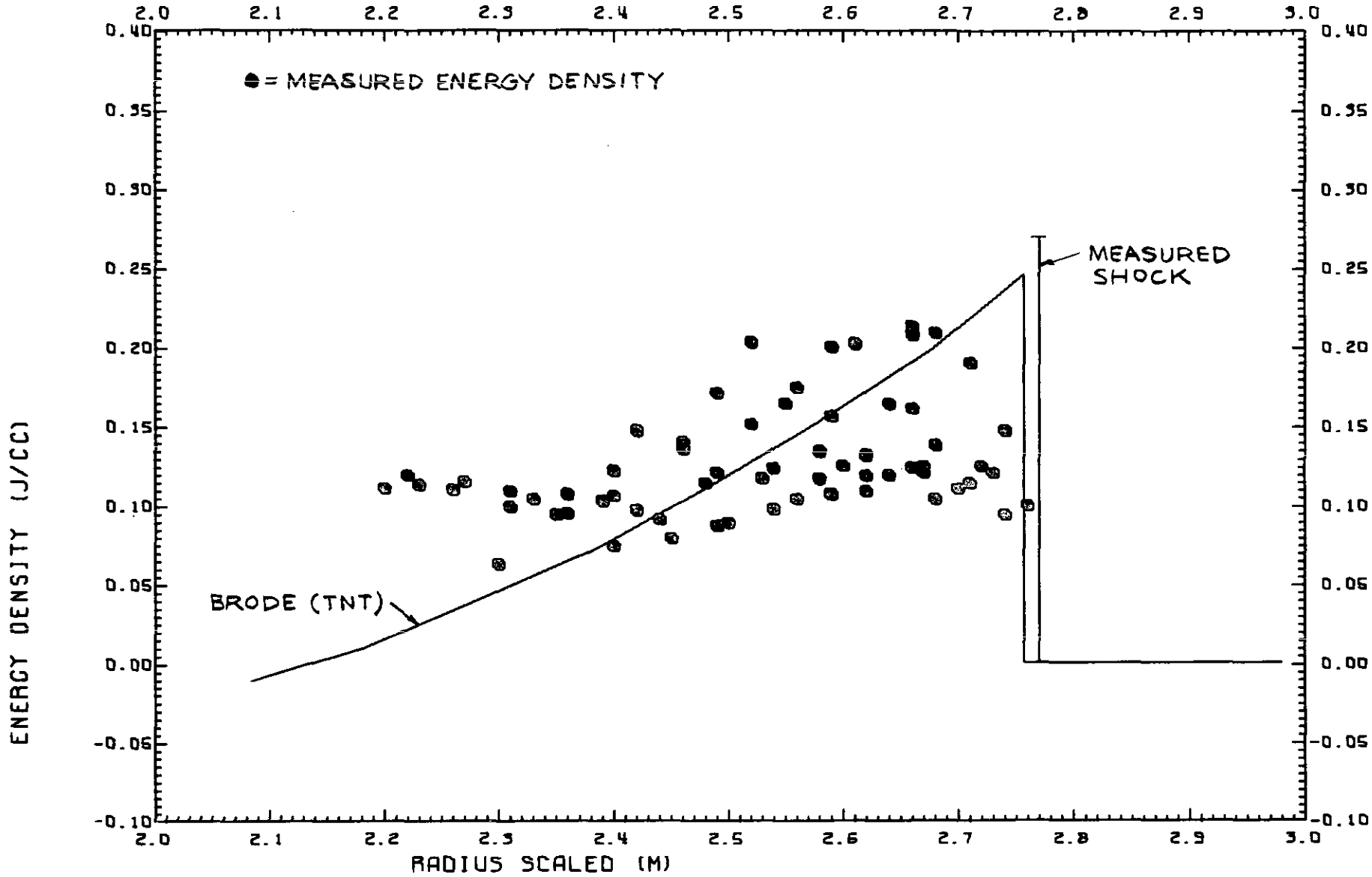

Figure 9 - Energy density in the primary wave, FE589/6 (t = 3.413 ms)

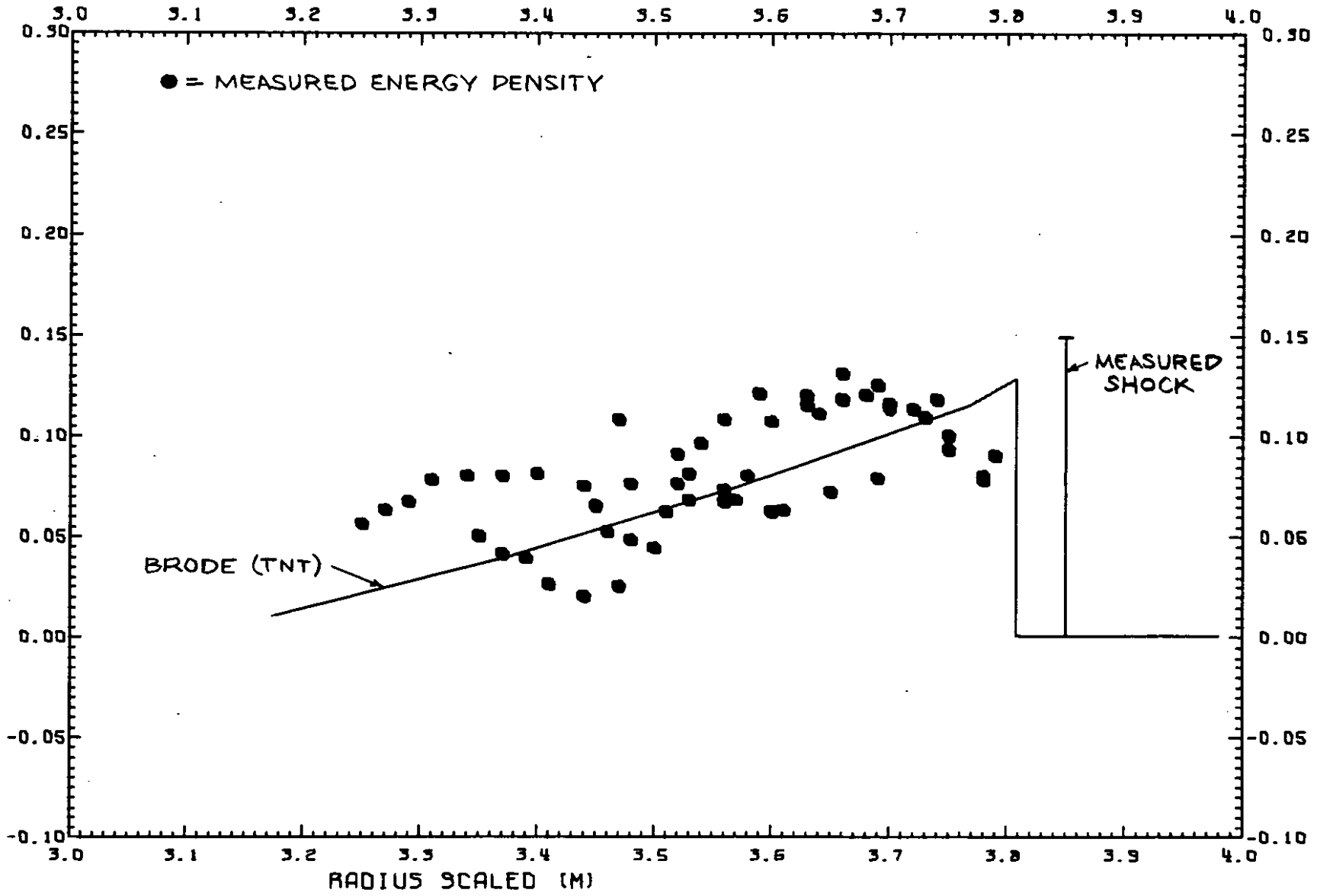

Figure 10 - Energy density in the primary wave, FE589/6 (t = 5.918 ms)

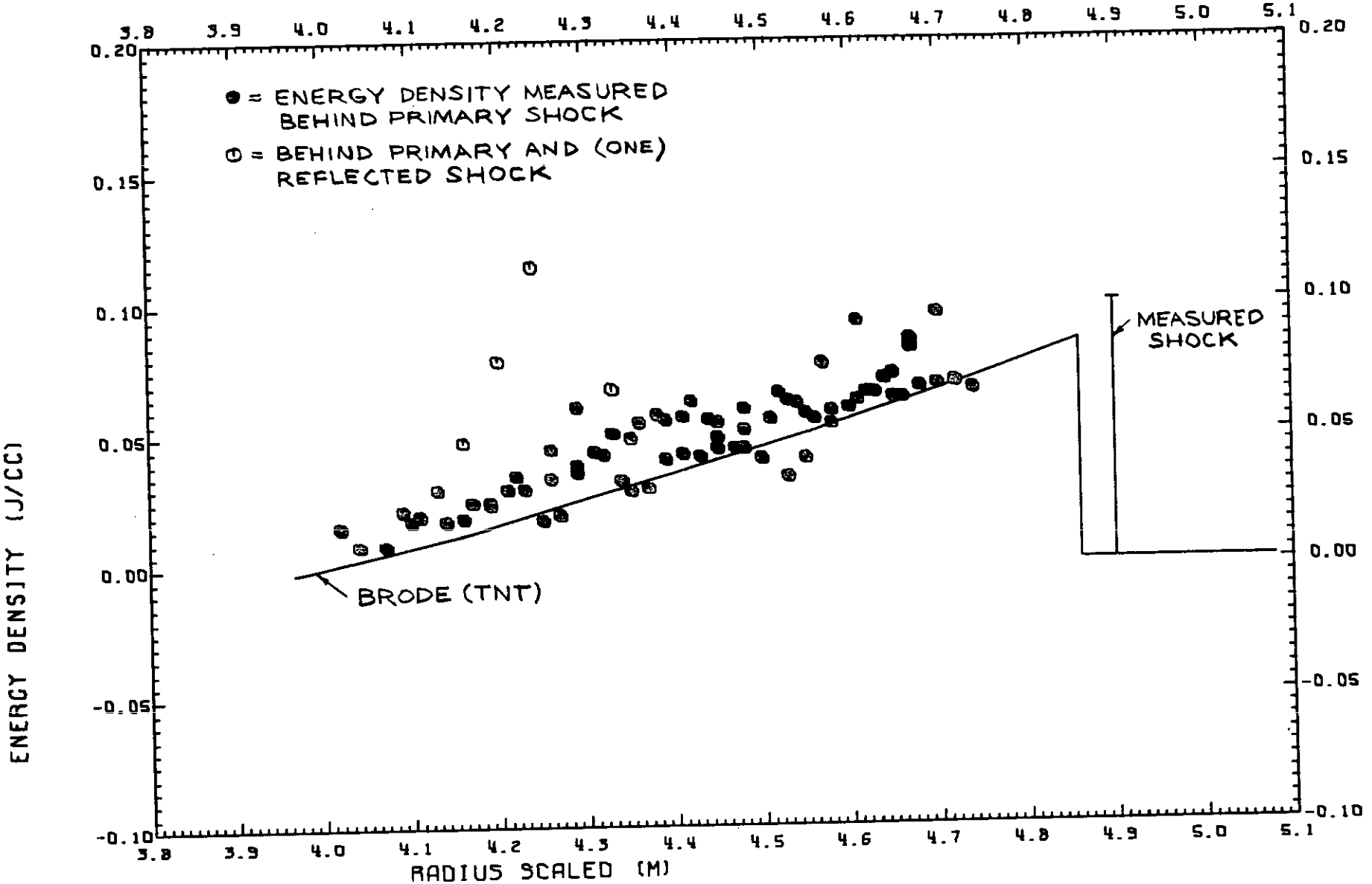

Figure 11 - Energy density in the primary wave, FE589/6 (t = 8.532 ms)

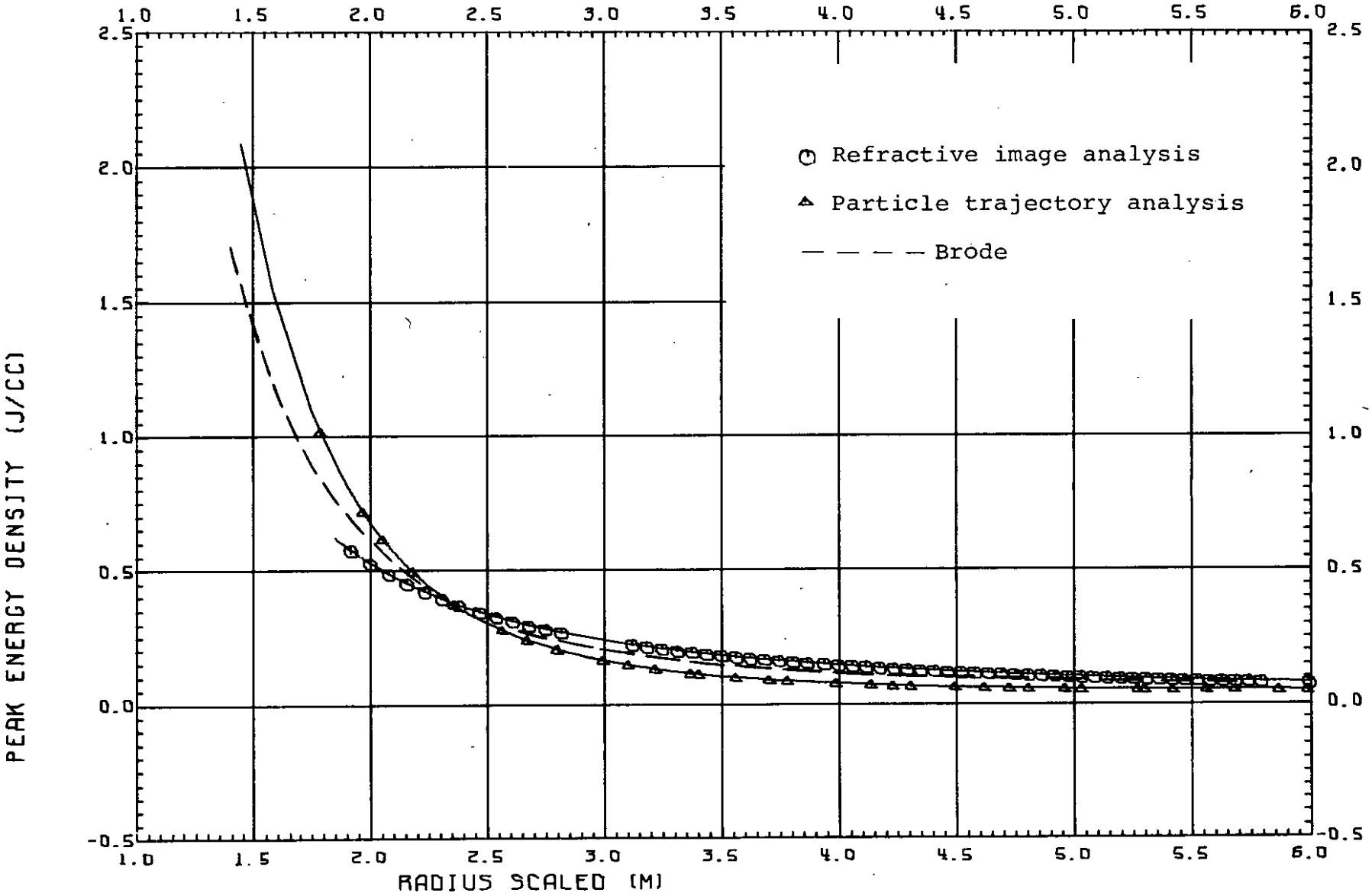

Figure 12 - Energy density at the primary shock front, FE589/6

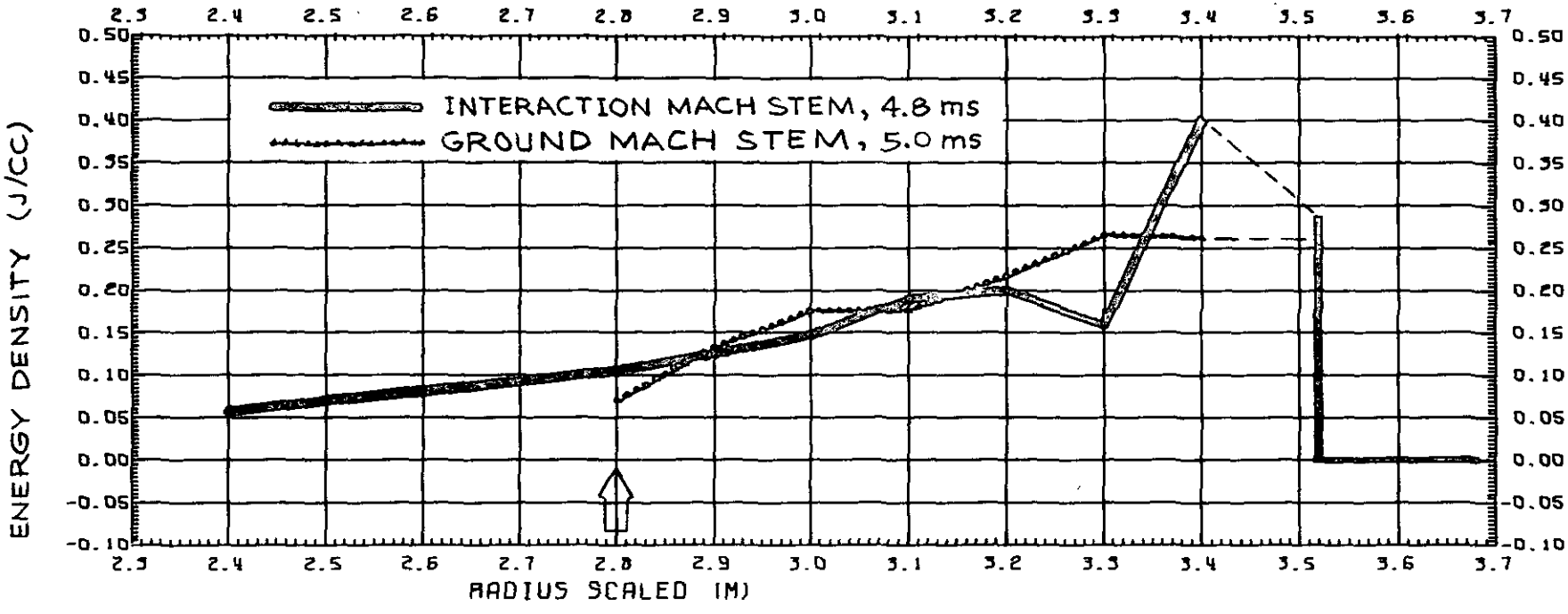

Figure 13 - Energy density profiles in the Mach stem regions, Dipole West/11 (R = 3.52 m)

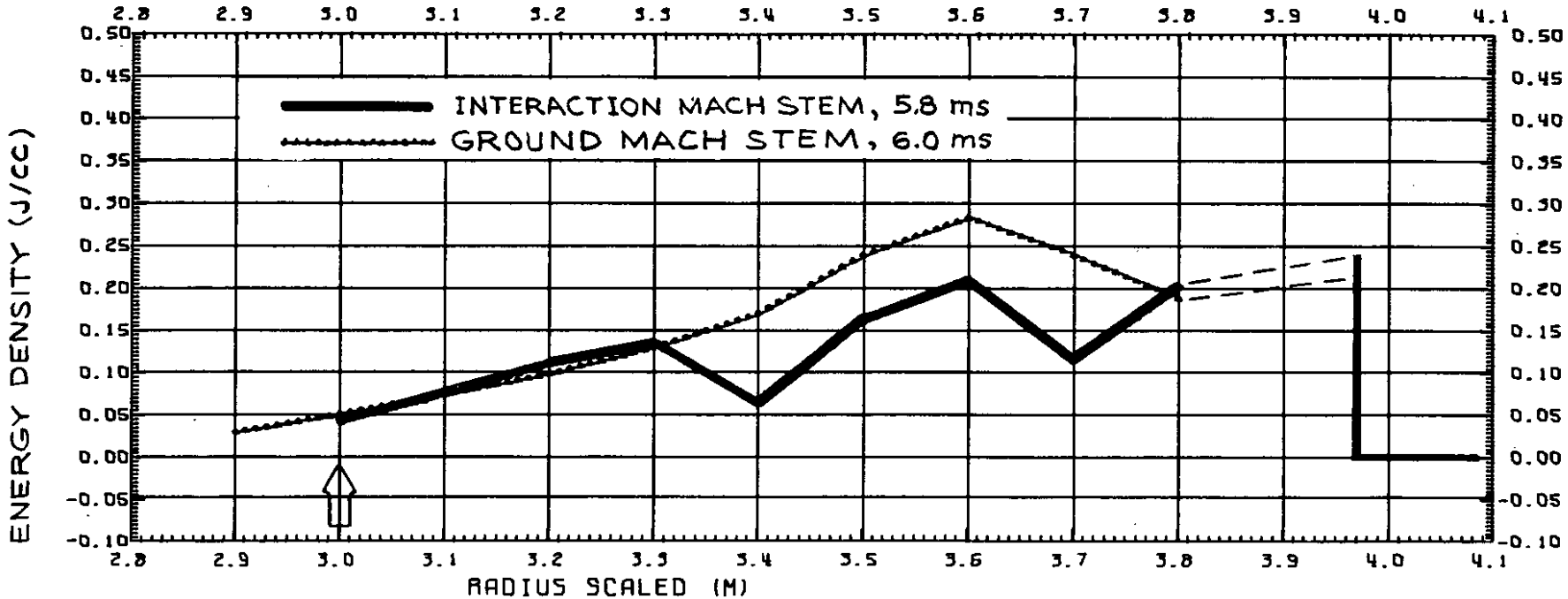

Figure 14 - Energy density profiles in the Mach stem regions, Dipole West/11 (R = 3.98 m)

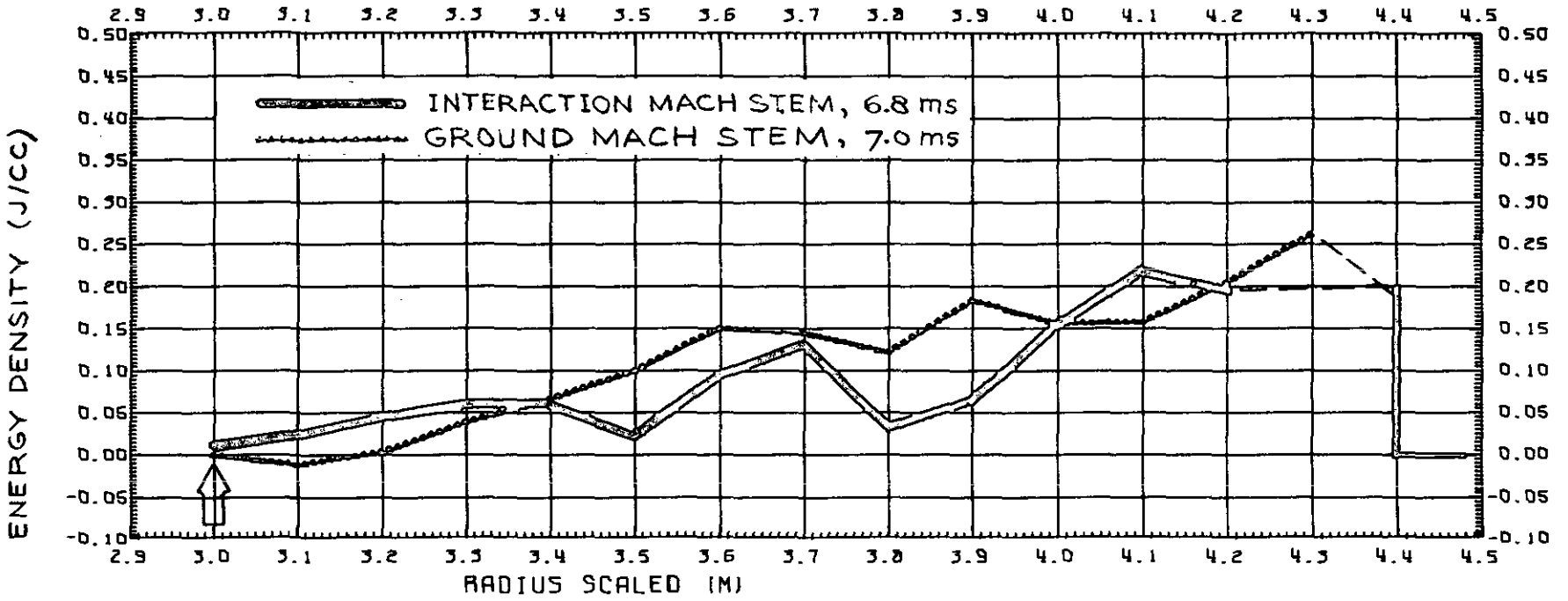

Figure 15 - Energy density profiles in the Mach stem regions, Dipole West/11 (R = 4.40 m)

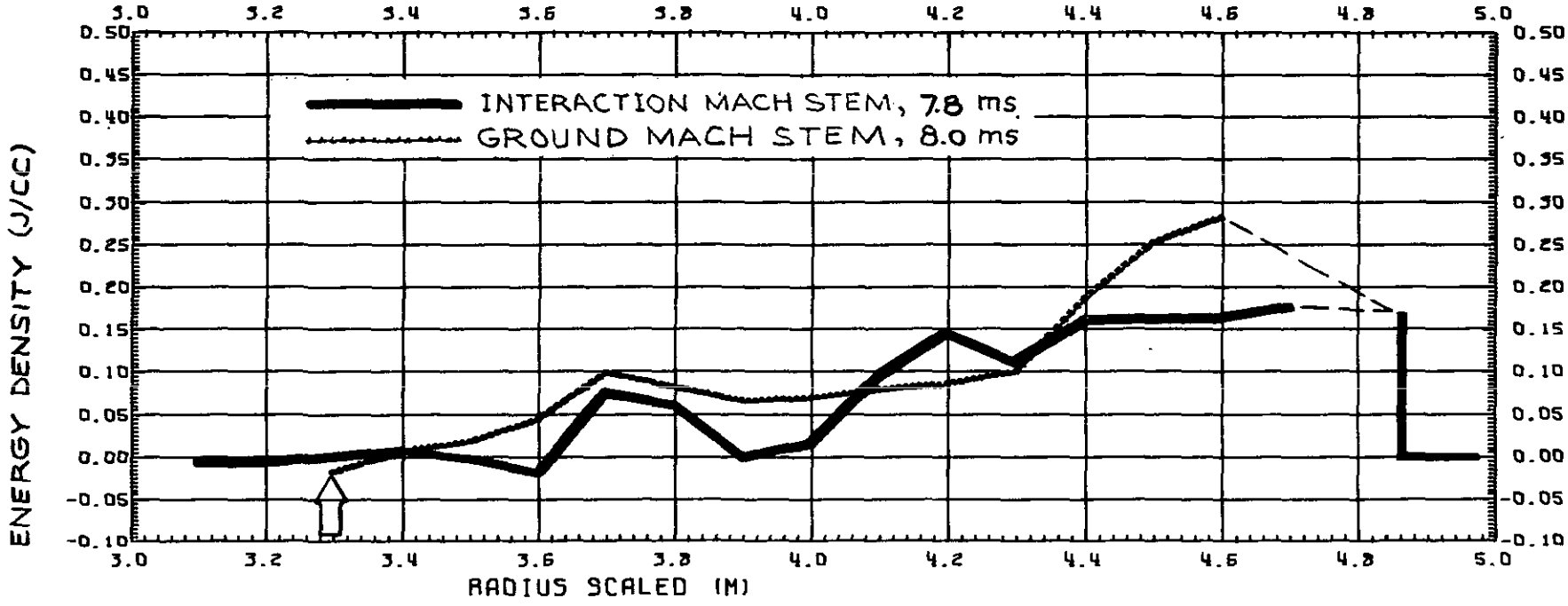

Figure 16 - Energy density profiles in the Mach stem regions, Dipole West/11 (R = 4.83 m)

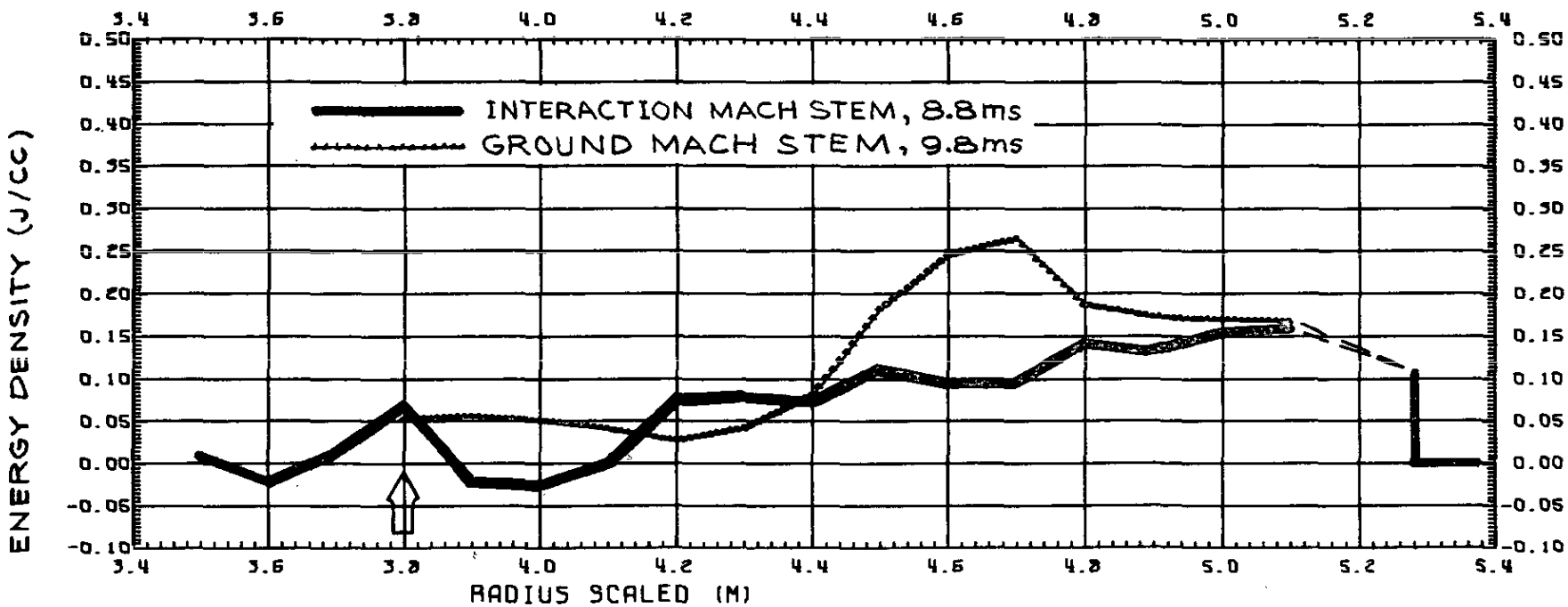
INTERACTION MACH STEM, 8.8ms
GROUND MACH STEM, 9.8ms
ENERGY DENSITY (J/CC)
RADIUS SCALED (M)
3.4
3.6
3.8
4.0
4.2
4.4
4.6
4.8
5.0
5.2
5.4
0.50
0.45
0.40
0.35
0.30
0.25
0.20
0.15
0.10
0.05
0.00
-0.05
-0.10

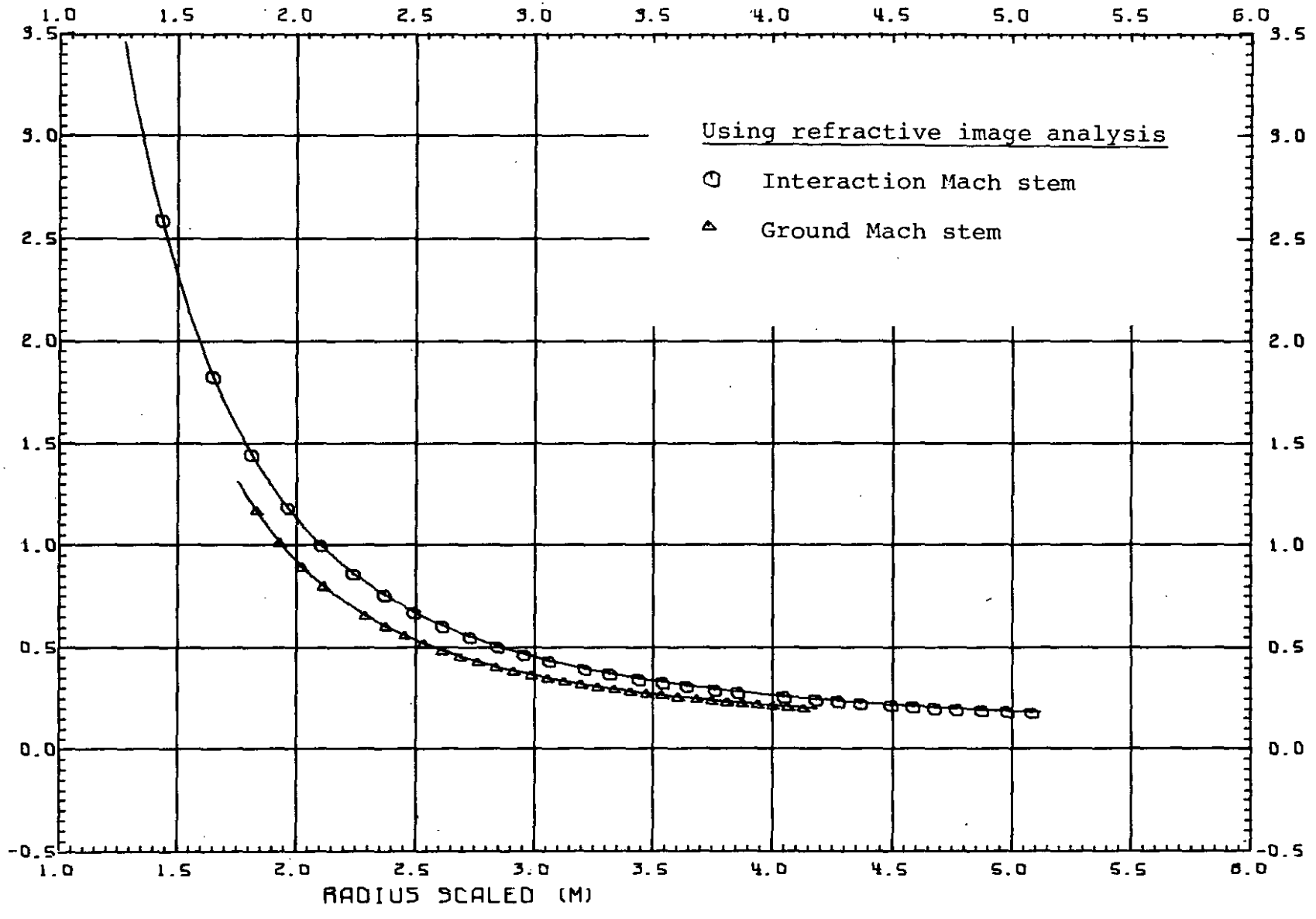

Figure 18 - Energy density at the Mach stem shock fronts, Dipole West/11 (RIA)

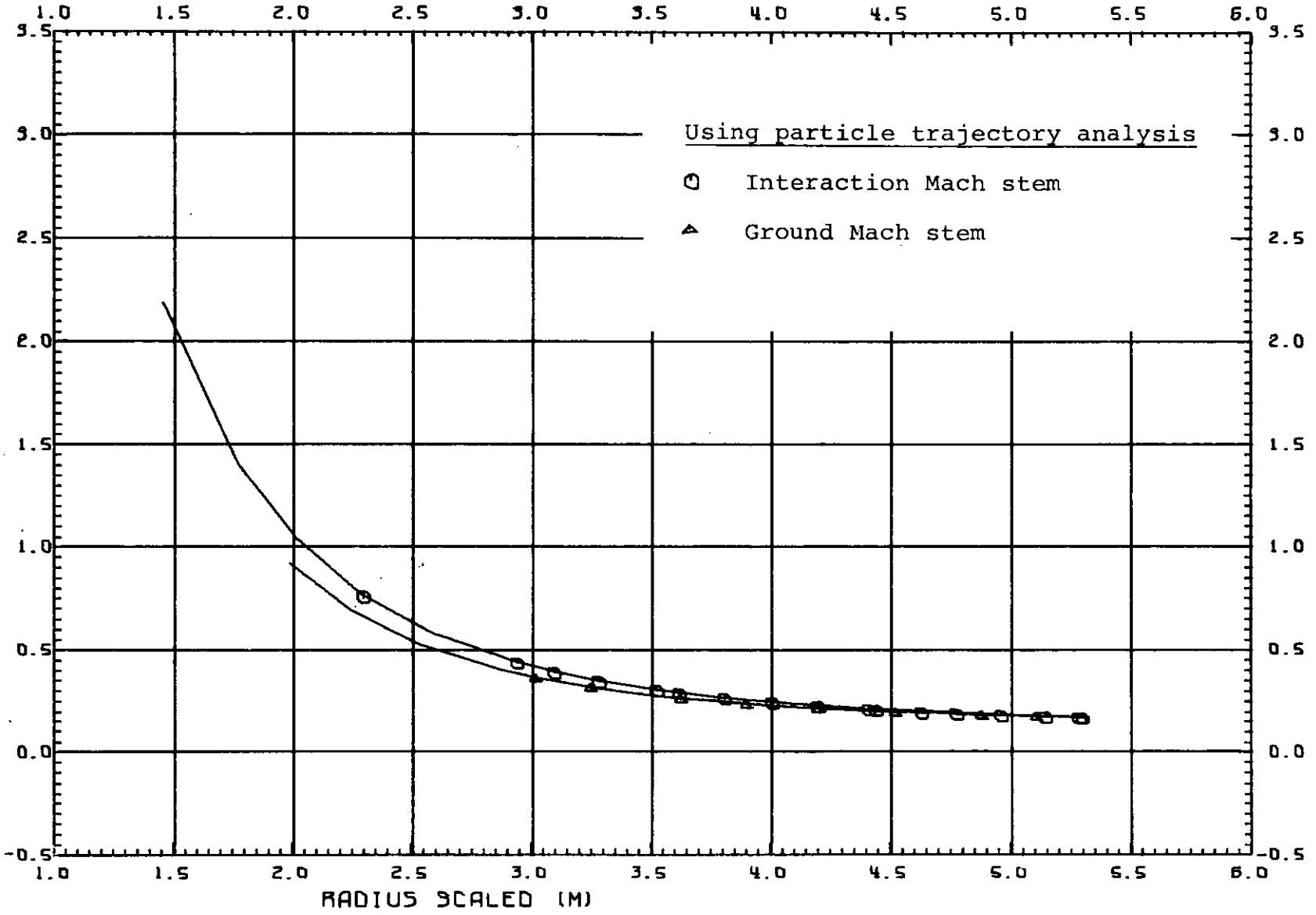

Figure 19 - Energy density at the Mach stem shock fronts, Dipole West/11 (PTA)

DISTRIBUTION LIST

No. of Copies	Organization
12	Commander Defense Documentation Center ATTN: DDC-DDA Cameron Station Alexandria, VA 22314
4	Director of Defense Research & Engineering ATTN: DD/TWP DD/S&SS DD/I&SS AD/SW Washington, DC 20301
3	Director Defense Advanced Research Projects Agency ATTN: Technical Library NMRO PMO 1400 Wilson Boulevard Arlington, VA 22209
6	Director Defense Nuclear Agency ATTN: STTL (Tech Lib, 2 cys) SPAS, Mr. J. Moulton DDST, Mr. P.H. Haas SPSS, Dr. George Ullrich SPAS, Mr. D. Kohler Washington, DC 20305
2	Commander Field Command, DNA ATTN: FCTMOF Kirtland AFB, NM 87115
2	Department of Defense Explosives Safety Board ATTN: R. Perkins Dr. Tom Zaker Room GS-270, Forrestal Bldg Washington, DC 20314
1	Commander US Army Materiel Development and Readiness Command ATTN: DRCDMD-ST 5001 Eisenhower Avenue Alexandria, VA 22333
1	Commander US Army Aviation Research and Development Command ATTN: DRSAV-E 12th and Spruce Streets St. Louis, MO 63166
1	Director US Army Air Mobility Research & Development Laboratory Ames Research Center Moffett Field, CA 94035
1	Commander US Army Electronics Research & Development Command Technical Spt Activity ATTN: DELSD-L Fort Monmouth, NJ 07703
1	Commander US Army Communications Research & Development Command ATTN: DRDCO-PPA-SA Fort Monmouth, NJ 07703
3	Commander US Army Missile R&D Command ATTN: DRDMI-R DRDMI-YDL DRDMI-S, Chief Scientist Redstone Arsenal, AL 35809
2	Commander US Army Tank Automotive Research & Development Command ATTN: DRDTA-UL DRDTA-RHT, LT P. Hasek Warren, MI 48090

DISTRIBUTION LIST

No. of Copies	Organization
2	Commander US Army Armament Materiel Readiness Command ATTN: SARRI-LR, B. Morris DRSAR-LEP-L, Tech Lib Rock Island, IL 61299
4	Commander US Army Armament Research & Development Command ATTN: DRDAR-TSS (2 cys) P. Angelotti Mr. Demitrack Dover, NJ 07801
4	Commander US Army Harry Diamond Lab ATTN: DRXDO-TI/012 DRXDO-NP, F. Wimenitz DRXDO-NP, J. Gaul DRXDO-NP, J. Gwaltney 2800 Powder Mill Road Adelphi, MD 20783
1	Director US Army Materials and Mechanics Research Center ATTN: Technical Library Watertown, MA 02172
1	Commander US Army Foreign Science and Technology Center ATTN: Research & Data Branch 220 7th Street, NE Charlottesville, VA 22901
3	Commander US Army Nuclear Agency ATTN: ATCN-W, CAPT M. Bowling CDINS-E Technical Library 7500 Backlick Road, Bldg 2073 Springfield, VA 22150
1	Director US Army TRADOC Systems Analysis Activity ATTN: ATAA-SL, Technical Lib White Sands Missile Range New Mexico 88002
1	HQDA (DAMA-AR, NCB Division) Washington, DC 20310
3	Director US Army Advanced BMD Technology Center ATTN: Mr. B.E. Kelley Mr. M. Capps Mr. Marcus Whitfield P.O. Box 1500 Huntsville, AL 35807
1	Commander US Army Ballistic Missile Defense Systems Command ATTN: SSC-DH, H. Solomonson P.O. Box 1500 Huntsville, AL 35807
1	Commander US Army Ballistic Missile Defense Program Office ATTN: DACS-SAE-S, J. Shea 5001 Eisenhower Avenue Alexandria, VA 22333
2	Commander US Army Engineer Waterways Experiment Station ATTN: Library W. Flateau P.O. Box 631 Vicksburg, MS 39180

DISTRIBUTION LIST

No. of Copies	Organization
2	Chief of Naval Research Department of the Navy ATTN: T. Quinn, Code 464 Technical Library J.L. Warner, Code 464 Washington, DC 20360
2	Commander Naval Ship Eng'g Center ATTN: J. R. Sullivan NSEC 6105-G Technical Library Hyattsville, MD 20782
4	Commander Naval Surface Weapons Center ATTN: Code 1224, Navy Nuclear Programs Office Code 241, J. Petes Code 730, Tech Library J. Pittman Silver Spring, MD 20910
1	Commander Naval Weapons Evaluation Fac ATTN: Document Control Kirtland AFB, NM 87117
1	Commander Naval Civil Engineering Lab ATTN: Dr. W. A. Shaw, Code L31 Port Hueneme, CA 93041
3	Director Naval Research Laboratory ATTN: M. Persechino G. Cooperstein Tech Lib, Code 2027 Washington, DC 20375
1	HQ USAFSC (DLCAW, Technical Lib) Andrews AFB Washington, DC 20331
1	AFOSR (OAR) Bolling AFB, DC 20332
1	RADC (Document Lib, FMTLD) Griffis AFB, NY 13440
4	AFWL (CA, Dr. A. Guenther DYT, Charles Needham DYT, MAJ G. Ganong; S. Melzer) Kirtland AFB, NM 87117
1	AFCRL L. G. Hanscom Field Bedford, MA 01730
1	SAMSO (Library) P.O. Box 92960 Los Angeles, CA 90009
3	AFTAC (K. Rosenlof R. McBride G. Leies) Patrick AFB, FL 32925
2	AFML (G. Schmitt, MAS; D. Schmidt) Wright-Patterson AFB, OH 45433
2	Energy Research & Development Administration Department of Military Application ATTN: R&D Branch Library Branch, G-043 Washington, DC 20545
2	Director Los Alamos Scientific Lab ATTN: Dr. J. Taylor Technical Library P.O. Box 1663 Los Alamos, NM 87554

DISTRIBUTION LIST

No. of Copies	Organization
1	Director, NASA ATTN: Code 04.000 Langley Research Center Langley Station Hampton, VA 23365
1	Director NASA Scientific & Technical Information Facility ATTN: SAK/DL P.O. Box 8757 Baltimore/Washington International Airport, MD 21240
1	National Academy of Sciences ATTN: Dr. Donald Groves 2101 Constitution Avenue, NW Washington, DC 20418
1	Aerospace Corporation ATTN: Tech Information Svcs. Bldg 105, Rm 2220 P.O. Box 92957 Los Angeles, CA 90009
1	Agbabian Associates ATTN: Dr. J. Malthan 250 N. Nash Street El Segundo, CA 90245
1	AVCO Government Products Group ATTN: Dr. W. Bade 201 Lowell Street Wilmington, MA 01887
1	AVCO-Everett Research Lab ATTN: Technical Library 2385 Revere Beach Parkway Everett, MA 02149
1	John A. Blume & Associates ATTN: Dr. John A. Blume Sheraton-Palace Hotel 100 Jessie Street San Francisco, CA 94105
1	CALSPAN Corporation ATTN: Library P.O. Box 235 Buffalo, NY 14221
1	Effects Technology, Inc. ATTN: E. Anderson 5383 Holister Avenue Santa Barbara, CA 93105
1	General Electric Co. — TEMPO ATTN: DASIAC 816 State Street, Drawer QQ Santa Barbara, CA 93102
10	General Electric Co. — TEMPO ATTN: Dr. Lynn Kennedy 7800 Marble Avenue, NE, Suite 5 Albuquerque, NM 87110
1	H-Tech Laboratories, Inc. ATTN: B. Hartenbaum P.O. Box 1686 Santa Monica, CA 90406
1	Hughes Aircraft Company Systems Development Laboratory ATTN: Dr. A. Puckett Centinela and Teale Streets Culver City, CA 92032
1	Ion Physics Corporation ATTN: Technical Library South Bedford Street Burlington, MA 01803
1	Kaman Sciences Corporation ATTN: Dr. C. Sachs 1500 Garden of the Gods Road Colorado Springs, CO 80907

DISTRIBUTION LIST

No. of Copies	Organization
1	Kaman Avidyne, Division of Kaman Sciences ATTN: Dr. J. Ray Ruetenik 83 2nd Ave, NW Industrial Park Burlington, MA 01803
1	KTECH Corporation ATTN: Dr. Donald V. Keller 911 Pennsylvania NE Albuquerque, NM 87110
1	Lockheed Missiles & Space Co, Inc. Division of Lockheed Aircraft Corp ATTN: J. Nickell P.O. Box 504 Sunnyvale, CA 94088
1	Management Science Associates ATTN: Kenneth Kaplan P.O. Box 239 Los Altos, CA 94022
1	Martin Marietta Aerospace Orlando Division ATTN: A. Ossin P.O. Box 5837 Orlando, FL 32805
1	Maxwell Laboratories, Inc. ATTN: A. Kolb 9244 Balboa Avenue San Diego, CA 92123
1	McDonnell Douglas Astronautics Corporation 5301 Bolsa Avenue Huntington Beach, CA 92647
1	Philco Ford Corporation Aeronutronic Division ATTN: L. K. Goodwin Newport Beach, CA 92663
2	Physics International Company ATTN: Document Control Fred Sauer 2700 Merced Street San Leandro, CA 94577
3	R&D Associates ATTN: Technical Library Jerry Carpenter Allen Kuhl P.O. Box 9695 Marina del Rey, CA 90291
1	Sandia Laboratories ATTN: Dr. J. Kennedy P.O. Box 5800 Albuquerque, NM 87115
2	Science Applications, Inc. ATTN: Mr. J. W. Miller Dr. John Cockayne 8400 West Park Drive McLean, VA 22101
1	Shock Hydrodynamics, Inc. ATTN: L. Zernow 4710-16 Vineland Avenue N. Hollywood, CA 91602
1	Systems, Science & Software ATTN: Technical Library P.O. Box 1620 La Jolla, CA 92036
1	Teledyne-Brown Engineering ATTN: Dr. M. Batel Research Park Huntsville, AL 35807
1	Union Carbide Corporation Oak Ridge National Laboratory ATTN: Technical Library P.O. Box X Oak Ridge, TN 37830

DISTRIBUTION LIST

No. of Copies	Organization
1	URS Research Company ATTN: Technical Library 155 Bovet Road San Mateo, CA 94002
1	Battelle Memorial Institute ATTN: Technical Library 505 King Avenue Columbus, Ohio 43201
2	Denver Research Institute University of Denver ATTN: Mr. John Wisotski P.O. Box 10127 Denver, CO 90210
1	Director Applied Physics Laboratory The Johns Hopkins University Johns Hopkins Road Laurel, MD 20810
1	Lovelace Research Institute ATTN: Dr. D. Richmond P.O. Box 5890 Albuquerque, NM 87108
1	Massachusetts Institute of Technology Aerophysics Laboratory Cambridge, MA 02139
1	New Mexico Institute of Mining and Technology ATTN: Mr. P. McClain Socorro, NM 87801
1	Northwestern Michigan College ATTN: Prof. D.C. Kennard, Jr. Traverse City, MI 49584

No. of Copies	Organization
1	Southwest Research Institute ATTN: Dr. W. Baker 8500 Culebra Road San Antonio, TX 78206
1	Stevens Institute of Technology Dept of Electrical Engineering ATTN: Prof. R. Geldmacher Castle Point Station Hoboken, NJ 07039
1	Research Institute of Temple University ATTN: Technical Library Philadelphia, PA 19144
1	Texas Tech University Dept of Civil Engineering ATTN: Mr. Joseph E. Minor Lubbock, TX 79409
1	University of Arkansas Department of Physics ATTN: Prof. O. Zinke Fayetteville, AR 72701
1	University of California Lawrence Livermore Laboratory Technical Information Division ATTN: Technical Library Dr. Donald N. Montan P.O. Box 808 Livermore, CA 94550
1	University of Illinois Consulting Engineering Services ATTN: Nathan M. Newmark 1211 Civil Engineering Building Urbana, IL 61801

DISTRIBUTION LIST

No. of Copies	Organization
1	University of Maryland Department of Physics ATTN: Dr. E. Oktay College Park, MD 20742
1	The University of Michigan Gas Dynamics Laboratory ATTN: Z. Gabrijel Aerospace Engineering Building Ann Arbor, MI 48109
1	University of New Mexico Eric H. Wang Civ Eng'g Res Fac ATTN: Technical Library University Station, Box 188 Albuquerque, NM 87131
1	University of Oklahoma Department of Physics ATTN: Prof. R. Fowler Norman, OK 73069

Aberdeen Proving Ground

Director, USAMSAA
ATTN: Dr. J. Sperrazza
Mr. R. Norman, GWD
DRXSY-MP, H. Cohen
Cdr, USATECOM
ATTN: DRSTE-SG-H
Director, Weapons System
Concepts Team
Bldg. E3516, EA
ATTN: DRDAR-ACW